

Estimation of evapotranspiration and its parameters for pine, switchgrass, and intercropping with remotely-sensed images based geospatial modeling

Sudhanshu Sekhar Panda^{a,*}, Devendra Man Amatya^b, Augustine Muwamba^c, George Chescheir^d

^a Institute for Environmental Spatial Analysis, University of North Georgia, 3820 Mundy Mill Road, Oakwood, GA, 30566, USA

^b Center for Forested Wetlands Research, USDA Forest Service, 3734 Highway 402, Cordesville, SC, 29434, USA

^c College of Engineering, University of Georgia, Athens, GA, 30602, USA

^d Department of Agriculture and Biosystems Engineering, North Carolina State University, Raleigh, NC, 27695, USA

ARTICLE INFO

Keywords:

ArcGIS ModelBuilder
Canopy temperature
Data mining
Evapotranspiration
Landsat
Orthoimagery
Python script
RBFN
Software development
Soil moisture
SPOT
Stomatal conductance
Visual basics studios

ABSTRACT

Intercropping switchgrass (*Panicum virgatum*) with pine can increase bioenergy feedstock production without land opportunity costs but can potentially alter water budgets. Measuring evapotranspiration (ET) and its parameters (stomatal conductance (g_s), leaf area index (LAI), canopy temperature (T_c), and soil moisture (SM)) across cropping systems is costly and time-consuming. However, interpretation of remotely-sensed data can facilitate the effective assessment of relative ET demands among competing forest landuses. This study develops and tests geospatial models informed by a normalized difference vegetation index (NDVI), soil adjusted vegetation index (SAVI), vegetation vigor index (VVI), and other spectral information to estimate ET and its parameters, which are measured on experimental watersheds with young pines and natural understory (YP), switchgrass only (SG), and young pine intercropped with switchgrass (IC). The treatment watersheds were replicated on three sites located across the Southeastern U.S. in Carteret, NC; Calhoun, MS; and Greene, AL. Despite the growth inconsistency for the SG only treatment, remote modeling estimation of ET parameters yielded an acceptable $R^2 > 0.70$, and the ET model yielded R^2 of 0.50 and a standard error of prediction of 0.94. However, ET and ET parameter model estimation for the IC performed somewhat less satisfactorily, with an R^2 of 0.47, 0.59, 0.56, 0.81, and 0.57 for ET, LAI, g_s , T_c , and SM, respectively, potentially due to inconsistencies in Landsat image pixel size and landuse homogeneity. Moreover, ET parameter models for the YP site performed rather poorly, with $R^2 = 0.28, 0.63,$ and 0.76 for LAI, g_s , and T_c , respectively. Additionally, image analysis automation was created with Python scripting and geospatial models. The findings from this study suggest that inclusion of more spatial variability, sound data mining, ultra-high resolution imagery and advanced image processing approaches to account for potential modeling uncertainties can enhance the predictive capability of models to remotely estimate environmental parameters including ET. Radial Basis Function Network (RBFN) based models provided promising results for estimating ET and ET parameters using remotely-sensed digital information when they are prepared with advanced data mining, but it is likely that laypersons may find these models difficult to use. However, forest managers with access to neural network software can use our devised RBFN training models for estimating those forest hydrologic parameters with better accuracy.

1. Introduction

The U.S. Department of Energy and the scientific community have a goal of producing biofuel from energy crops such as switchgrass (*Panicum virgatum*), a cheaper alternative to row crops or other agricultural commodities like corn, sweet sorghum, sugarcane, sugar beet, crop residues, and other woody biomass. Although crop residues and other woody biomass are abundantly available and much cheaper to

procure than switchgrass, they have their own downsides. Crop residues, one source of soil organic carbon, are essential for soil fertility enhancement and useful for soil erosion control, increased water infiltration, and evapotranspiration (ET) reduction, but need to be left in the field and tilled to provide a positive effect on crop production (Lal, 2004; Jarecki and Lal, 2003). In their review of next-generation biomass feedstock for biofuel production, Simmons et al. (2008) discussed the constraints of biofuel production from woody biomass and other

* Corresponding author.

E-mail addresses: Sudhanshu.Panda@ung.edu (S.S. Panda), damatya@fs.fed.us (D.M. Amatya), amuwamba@uga.edu (A. Muwamba), cheschei@eos.ncsu.edu (G. Chescheir).

<https://doi.org/10.1016/j.envsoft.2019.07.012>

Received 11 March 2019; Received in revised form 15 July 2019; Accepted 18 July 2019

Available online 19 August 2019

1364-8152/ © 2019 Published by Elsevier Ltd.

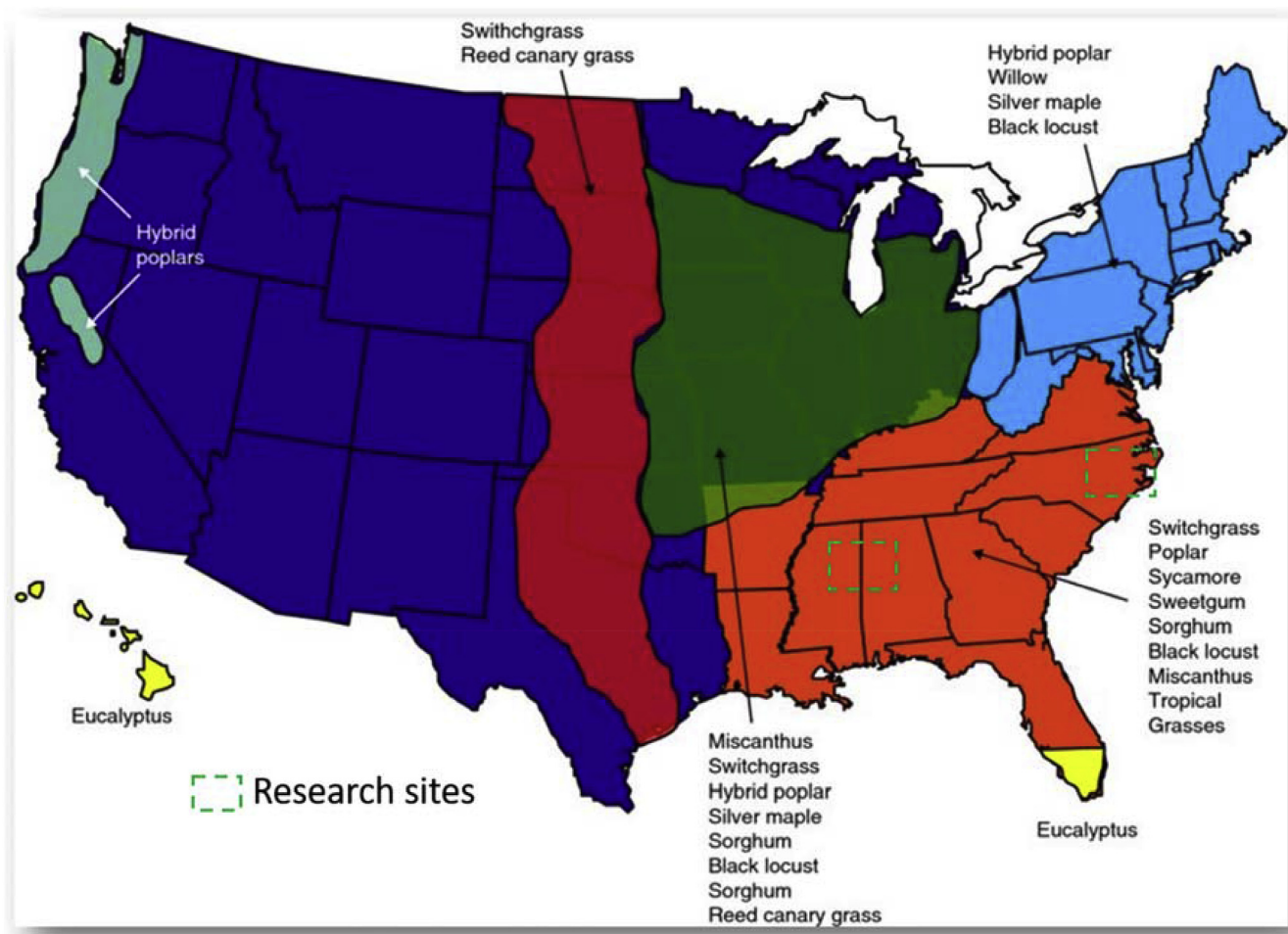


Fig. 1. Spatial locations suitable for growing perennial herbaceous species like switchgrass in United States (modified from Simmons et al., 2008).

agricultural products. They suggested that the use of dedicated herbaceous perennial crops such as switchgrass (Perrin et al., 2008; Parrish and Fike, 2005), miscanthus (Sahoo et al., 2018), and sorghum (Paterson et al., 2008) would be better alternatives. These herbaceous species can be grown in various regions of the United States (U.S.) (Fig. 1). Simmons et al. (2008) recommended switchgrass cultivation as an understory in the row-crop pine forests that are abundant in the Southeastern United States.

Pine plantations, which constitute the plurality of croplands in vast areas across the Southeastern United States from Mississippi to North Carolina, are managed to produce lumber, fiber for pulp, paper, cardboard, and bioenergy feedstocks. On a traditional pine plantation, the space between rows has no economic value. Grasses that can serve as bioenergy feedstocks, such as switchgrass, could be intercropped between rows in pine plantations and grown until the closing canopy of the pines shades them out. However, such intercropping raises environmental and ecological questions regarding the water budgets of forest plantations: Is the evapotranspiration (ET) of intercropped stands additive such that total ET can be estimated based on pine and switchgrass ET rates based on their relative coverage, or does intercropping cause competition for water between the two crops such that the total ET is less than the sum of ET expected from the individual crops? These questions have implications for regional water budgets under potential bioenergy development scenarios, and for decisions about managing forestlands. This study is part of a larger study examining how the establishment of these cropping systems affects stream flows, surface and soil water quality, and water budgets.

As discussed, the addition of switchgrass understories in forest

plantations like row pine would have ecological consequences, especially if the switchgrass competes for soil water with the main forest crop. Using a soil-plant-atmosphere model parameterized with site-specific data, Albaugh et al. (2014) found increased ET in the intercropped sites when compared to the mature pine or switchgrass only plots. However, the watershed-scale ET comparison data are lacking for switchgrass intercropping versus natural understory intercropping in pine forests. Therefore, it is essential to quantify the amount of soil water used by switchgrass compared to row pine understories on a watershed scale.

Plant and soil/understory litter evaporation and transpiration (or evapotranspiration, ET) are major components of the hydrological cycle. Jaramillo and Destouni (2015) studied 100 basins for 'actual ET' (AET)/P variation with respect to flow regulation and irrigation impact and found a relatively large AET/P increase in water-limited basins, including for a major portion of those basins in the United States. Global land-cover changes impact the terrestrial water cycle. ET has a direct impact on hydrology, crop growth, and biomass production. Forest cover alteration, including intercropping to accommodate switchgrass, may change the ET and water balance of these forest ecosystems. Sterling et al. (2013), through their extensive study of 1500 estimates of annual evapotranspiration and corresponding global land-cover change database, projected a 5 percent decrease of global scale terrestrial evapotranspiration (TET) from the current anthropogenic land-cover change, mostly deforestation, and an increase in TET with forest cover intensification. An accurate estimation of ET and its spatial and temporal distribution is of key importance for hydrological and meteorological applications including regional-scale water balance

(Sun et al., 2011). The ET rate of any ecosystem depends upon soil moisture and vegetation factors as well as climatic variables like air and canopy temperature, radiation, vapor pressure, wind speed, and the physical characteristics of the evaporating surface (Viessman and Lewis, 2003). While plant evaporation occurs mostly from above-canopy interception as a function of canopy storage capacity and density (Amatya et al., 1996), understory/litter transpiration occurs by uptake and transport of water from the soil/aquifer system by plant roots, branches, stems, and eventually diffusing from plant leaves into the atmosphere (Senay et al., 2013).

ET estimation from the forest cover would provide insight to the soil water use by different crops, but it is a very cumbersome in situ-based approach. Rapid, accurate, and cost-effective estimation of ET and its supporting parameters, such as stomatal conductance (g_s), leaf area index (LAI), canopy temperature (canopy albedo - T_c), soil moisture (SM), and estimation of wind speed using remote-sensing technology has become increasingly popular (Panda et al., 2016). LAI is defined as the single-sided surface area of leaves per unit area of soil ($m^2 m^{-2}$) and is a key parameter implicit in a variety of forest ecosystem processes, including light and rain interception, transpiration, photosynthesis, and soil heterotrophic respiration (le Maire et al., 2006). LAI is a seasonal parameter and is an indicator of crop growth, thus ET and LAI correlate very well (Sun et al., 2011). LAI was also one of the hydrologic parameters recently discussed in parameterization guidelines and considerations for hydrologic models by Malone et al. (2015). Optical indirect methods (e.g., model LAI-2200 Plant Canopy Analyzer, LI-COR, Lincoln, NE) or hemispherical photographs and semi-direct methods using litter collection and allometric methods are used for local estimation of LAI (Brauman et al., 2012; le Maire et al., 2006; Malone et al., 2015; Panda et al., 2016), but these methods are time-consuming, cumbersome, and costly. According to Hilker et al. (2013), transpiration is directly linked to stomatal conductance (g_s). Local measurement of stomatal conductance is conducted by an indirect optical measurement (Malone et al., 2015) or by a semi-direct method using a vapor pressure deficit algorithm (Pearcy et al., 1989; Sampson et al., 2011), but these methods are also costly and time-consuming. Stomatal conductance of pine needles has been measured and used for estimating and modeling transpiration of pine forests (Amatya et al., 1996; Sack and Scoffoni, 2012). Hilker et al. (2013) suggested that satellite retrievals of photosynthesis or gross primary production (GPP) could be used to quantify transpiration rates through g_s (Amatya and Skaggs, 2001). Canopy conductance (g_c) is generally approximated as a product of g_s and LAI (Amatya and Harrison, 2016; Amatya et al., 1996; Brauman et al., 2012; Amatya and Skaggs, 2001; Jensen et al., 1990; Nghi et al., 2008; Panda et al., 2014; Tian et al., 2012) although the maximum stomatal conductance also may be estimated as a function of measured ET, vapor pressure deficit, and other environmental variables (Morris et al., 1998), as will be shown below. Canopy temperature can serve as a surrogate for the amount of evaporation and transpiration through the plant canopy and can be estimated with direct measurement using thermometers (Bastiaanssen et al., 1998). Forest soil moisture is generally estimated through instrumentation using a tensiometer and lysimeter (Olivera-Guerra et al., 2015; van der Ploeg and de Rooij, 2014; Vasquez et al., 2015).

Routine in-situ measurement of plant hydrologic parameters is time-consuming and expensive (Panda et al., 2014; Sampson et al., 2011). Majasalmi et al. (2017) have a detailed review of the comparison of optical and allometric field instrumentation for forest hydrologic parameter estimation and are in favor of optical remote sensing approaches. Estimating forest ET using remote sensing data is not a new concept. There are many successful examples of using remotely-sensed images to model ET and water budgets for grasslands and crop lands (Chen et al., 1997; Feddema and Eggebert, 2005; Johnson, 2016; Noori and Panda, 2016; Panda et al., 2009; Rao et al., 2006; Schellberg et al., 2008; Tian et al., 2013; Turner et al., 1999; Wang and Jia, 2013), but such models have limitations for forests, especially for understory in-

between forest rows, as the satellites cannot “see” the ground or the understory in closed canopy forests, and thus cannot sense either soil moisture or the spectral characteristics of the understory (Panda et al., 2002; Pisek et al., 2015, 2016; Yang et al., 2014a,b; 45–47).

Li and Lyons (2002) used 1.1 km resolution NOAA-14 AVHRR remote sensing data to derive surface temperature, which was combined with limited routine meteorological data like soil moisture to estimate the ET rates in central Australia with limited success. Cristobal and Poystos (2011) tested the reliability of remote sensing data of TERRA and LANDSAT to estimate forest vegetation ET in the Vallcebre research catchment in Spain from 2003 to 2005 using 27 AQUA-MODIS images, 11 Landsat-7, and 10 Landsat-5 images in comparison with stand transpiration obtained from sap flow measurements. However, even the best estimations of forest ET obtained from Landsat images had 30 percent uncertainty (Cristobal and Poystos, 2011). Panda et al. (2018) used cloud-free Landsat images from 2006 to 2014 and an advanced data mining approach to obtain principal component bands to correlate with ET data. They obtained a strong correlation between the remote digital information and the ET of pine forest with a model R^2 of 0.58. They (Panda et al., 2018) used Backpropagation Neural Network (BPNN) and Radial Basis Function Network (RBFN) models and obtained a testing/validation average absolute error of 0.18 and 0.15 Wm^{-2} , and an average accuracy of 81 and 85 percent, respectively.

The thermal band of Landsat satellite imagery can be used to estimate canopy temperature (Lee, 1994; Panda et al., 2016; Senay et al., 2013). Satellite-imagery approaches are generally based on the principles of the surface-energy balance, exploiting the remotely derived land-surface temperature as a proxy indicator of surface-water status (Cammalleri et al., 2013). A review article by Wang and Qu (2009) explains how numerous studies have been conducted on the remote estimation of soil volumetric water content by using satellite, aerial, or simple digital photographic image analysis. Recent studies show that remotely-sensed data, especially freely available 30-m spatial resolution, 16-day temporal resolution Landsat Thematic Mapper (TM) images, can be used to efficiently estimate g_s , canopy temperature, LAI, and ET of forest vegetation (Carter, 1998; Curran, 1980; Hafeez et al., 2002; Justice et al., 1998; le Maire et al., 2006; Moran et al., 1994; North, 2002; Nouri et al., 2012; Olioso et al., 1999; Panda et al., 2016; Provoost et al., 2005; Rouse et al., 1973; Senay et al., 2013).

According to Liou and Kar (2014) and Panda et al. (2016, 2018), traditional approaches for ET estimation, such as weighing lysimeter, surface energy balance (SEB), Energy Balance Bowen Ratio (EBBR), eddy covariance techniques, pan-measurement, sap flow, scintillometer, water balance, etc., are mainly complex models and can estimate ET on local, field, and landscape scales only over a homogeneous vegetation cover with high accuracy. However, such approaches cannot be directly extended to estimate the ET rate of large areas of forest cover that contains natural heterogeneity and involves complex hydrologic processes, due to costly and time-consuming instrumentation processes (Idso et al., 1975; Panda et al., 2016; Zhang et al., 2016). Remotely-sensed image data is being used for mapping regional- and meso-scale patterns of ET and surface temperature, which is helpful in establishing a direct link between surface radiances and energy balance components (Caselles et al., 1992; Glenn et al., 2007; Idso et al., 1975; Kustas and Norman, 1996; Li et al., 2009; Long and Singh, 2013; Moran et al., 1989; Panda et al., 2016, 2018; Weigand and Bartholic, 1970; Yang and Shang, 2013; Zhang et al., 2016). Information embedded in satellite visible, near-infrared, middle infrared, and thermal infrared bands can be used to retrieve the land surface temperature (LST), vegetation index, and atmospheric temperature, and in turn supports ET estimation for large spatial extents and with higher temporal frequencies (Liou and Kar, 2014; Panda et al., 2016, 2018; Zhang et al., 2016).

These studies clearly show that the remote-sensing approach for estimating forest ET and its contributing parameters has strong appeal since it eliminates laborious, time-consuming, costly field methods,

which also have limitations in covering large areas and land cover heterogeneity (Majasalmi et al., 2017; Panda et al., 2016, 2018). The use of freely available moderate spatial resolution (30-m) Landsat data (Albaugh et al., 2014; Senay et al., 2013) and five other even lower resolution global fractions of absorbed Photosynthetically Active Radiation (fPAR, in the wavelength region of 400–700 nm) products like MODIS, MISR, MERIS, SeaWiFS, GEOV1 (250 m - ~1.1 km) has merit in estimating forest hydrologic parameters (Majasalmi et al., 2015; Tao et al., 2015; Verger et al., 2015; Yang et al., 2014a,b) covering large spatial extents. However, one problem that has not yet been documented is that pine/switchgrass intercropping widths (~3 m) cover areas smaller than the pixel scale (30-m) of Landsat 7 and 8 images.

This study addresses the methodological question of whether remotely-sensed spectral bands can be useful for modeling evapotranspiration and its components for young loblolly pine with a recruited understory, switchgrass, and its intercropping between young pine beds and explain the amount of water use by landuse types: 1) pine plantations intercropped with switchgrass and pine plantations intercropped with understories. The goal of this study was to develop and test object-oriented software to estimate the g_s , T_c , SM, LAI, and ET values of pine, switchgrass, and pine intercropped with switchgrass as well as understory. The specific objectives of the study were to develop:

1. Multivariate regression models using remotely-sensed imagery based digital information as predictor variable to estimate the g_s , T_c , SM, LAI, and ET, respectively, as outcome variables.
2. Artificial Neural Networks (ANN) models using remotely-sensed imagery based digital information RBFN algorithms to predict homogenous pine and switchgrass ET and the ET of pine intercropped with switchgrass as well as understory, respectively.
3. Executable software using the multivariate regression analyses-based algorithms, automated geospatial models, and Python scripts for endusers to apply for their application and usage.

2. Materials and methods

2.1. Study sites description

The sites included in this research are environmentally diverse: i) Carteret, NC (a topographically flat, well-managed coastal forest) (Fig. 2a); ii) Calhoun, MS (an upland inland forest with microtopography (Fig. 2b); and iii) Greene, AL (a moderate to steep sloped inland old forest ecosystem) (Fig. 2c). All three sites were established to investigate the environmental sustainability of intercropping switchgrass as a cellulosic biofuel between pine tree rows without using the land for food inside a managed pine forest owned and managed by Weyerhaeuser to produce timber, wood fiber, and biofuel feedstock (Bennett et al., 2013; Muwamba et al., 2015). Each site has a minimum of four watersheds with four distinct vegetation treatments, i) mature row-crop pine only; ii) young pine and switchgrass intercropping (6 m spacing between pine beds with ~ 3m for switchgrass); iii) pine and understory intercropping (6 m spacing between pine beds with ~ 3m for switchgrass); and iv) switchgrass only (Fig. 3). Each of the sites in Greene County, AL and Calhoun County, MS has an additional reference watershed with a mid-rotation pine forest not shown in Fig. 2.

The experimental watersheds, D0, D1, D2, and D3, in Carteret County, NC (34°49' N, 76°40' W) are 26.0, 26.3, 25.9, and 27.1 ha, respectively (Fig. 2). D0 is the watershed with young pine mixed with understory, D1 is a watershed with pine intercropped with switchgrass, D2 has mid-rotation thinned pine with a natural understory as a reference, and the fourth watershed, D3, is switchgrass-only. The northern, southern, and western sides of the study site are fully covered by forest, and the east side is dominated by agricultural land. The Carteret site topography is characterized by flat coastal plain at a 0.1 percent gradient and is at 3-m elevation above mean sea level (McCarthy et al., 1991). Deloss fine sandy loam soil; a fine-loamy,

mixed, thermic Typic Umbraquult that has poor drainage with shallow water tables and a pH range of 3.5–4.5 (acidic) represents the soil of the Carteret study site (Amatya et al., 1998; Beltran et al., 2010). The long-term mean annual precipitation and Penman-Monteith grass-reference evapotranspiration at the study site are 1517 mm and 1010 mm, respectively (Amatya and Skaggs, 2011).

In Greene County, Northwest Alabama, there are five watersheds (Fig. 2c) labeled GR1 (GR stands for Greene County), GR2, GR3, and GR4 with areas of 11.6, 26.7, 25.9, and 16.5, respectively, and a reference site (GRREF) that measures 6.8 ha (Bennett et al., 2013). By 2014, 6-year-old matured pine stands with understories were established in GR1. That same year, GR2 also had a 6-year-old young pine stand with understory, and GR3 had 8-yr old pine and switchgrass intercropping. Only switchgrass was grown in the GR4 watershed, and GRREF, not used in the study, contained 20-yr old mid-rotation matured pine. The soils in the watersheds are a combination of Falaya fine sandy loam, thermic Aeric Fluvaquent (somewhat poorly drained with a water table within 20 inches; slopes from 0 to 2 percent), Magnolia fine sandy loam, mesic Typic Pleudalf (well drained with slopes from 0 to 25 percent), and Shatuba fine sandy loam, thermic Typic Paleudult (well drained with slopes from 1 to 12 percent) (Bennett et al., 2013). The erosion risk on the watersheds varied from high on GR1 to low on GR3 and GR4. The slope of the site watersheds varies from 9.9 to 12.7 percent. The drainage at the outlets was measured using a flow meter located within a flume structure designed using the WINFLUME design program. The average PET of the watersheds varies from 1322 to 1471 mm, while the PET of the GRREF reference watershed was ~1600 mm (Bennett et al., 2013). Average annual precipitation of the Greene County site was 1361 mm.

In Calhoun County, MS, there are also five watersheds (Fig. 2b), labeled BF1 (BF stands for Befontaine), BF2, BF3, BF4, and BFREF (not shown in the figure and not used in the study) with areas of 14.1, 12.8, 10.9, 15.2, and 12.6 ha, respectively. By 2014, BF1 was a 7-yr old young pine stand with natural understory, BF2 was a pine stand thinned in 2007 with switchgrass intercropping, BF4 was a 8-yr old pine also intercropped with switchgrass, and BF3 was switchgrass only. BF5 was a mid-rotation pine stand planted in 1995. The soils at the site are a combination of Cuthbert fine sandy loam, thermic Typic Hapludult (well drained with a water table at or below 2 m; slopes 8 to 25 percent), Dulac silt loam, thermic Oxyaquic Fragiudalf (well drained with a water table at or below 2 m; slopes 0 to 12 percent), Ruston fine sandy loam, thermic Typic Paleudults (well drained with a water table at or below 2 m; slopes 0 to 8 percent), Providence silt loam, thermic Oxyaquic Fragiudalf (moderately well drained with a water table around 0.5 m; slopes 0 to 15 percent), Waverly silt loam, thermic Fluvaquentic (poorly drained with a water table from the surface to 0.4 m; slopes 0 to 2 percent), and Gullied Land. Half of the soils are classified as severely eroded. Drainage at the outlets was measured using a flow meter located within a flume structure designed using the WINFLUME design program. The site has an annual average temperature, precipitation, and potential evapotranspiration of 16.5 °C, 1405 mm, and 1350 mm, respectively.

2.2. Instrumentation and field data collection

2.2.1. Field ET calculation procedure

At all of the study sites, weather data were collected every 15 min by weather stations fitted with HOBO U30 Cellular Data Logger (Onset, Cape Cod, MA, USA), which were located in the proximity of the switchgrass only watersheds. The weather data collected for analyses in this study included precipitation (mm), atmospheric pressure (kPa), solar radiation ($W.m^{-2}$), wind speed ($m.s^{-1}$), gust speed ($m.s^{-1}$), wind direction, temperature (°C), and relative humidity (%). Each watershed was equipped with Decagon soil moisture probes (Model: 5TM) connected to a Campbell Scientific data logger (Model: CR200) at four depths (15 cm, 30 cm, 60 cm, and 80 cm) on the beds in tree rows and in

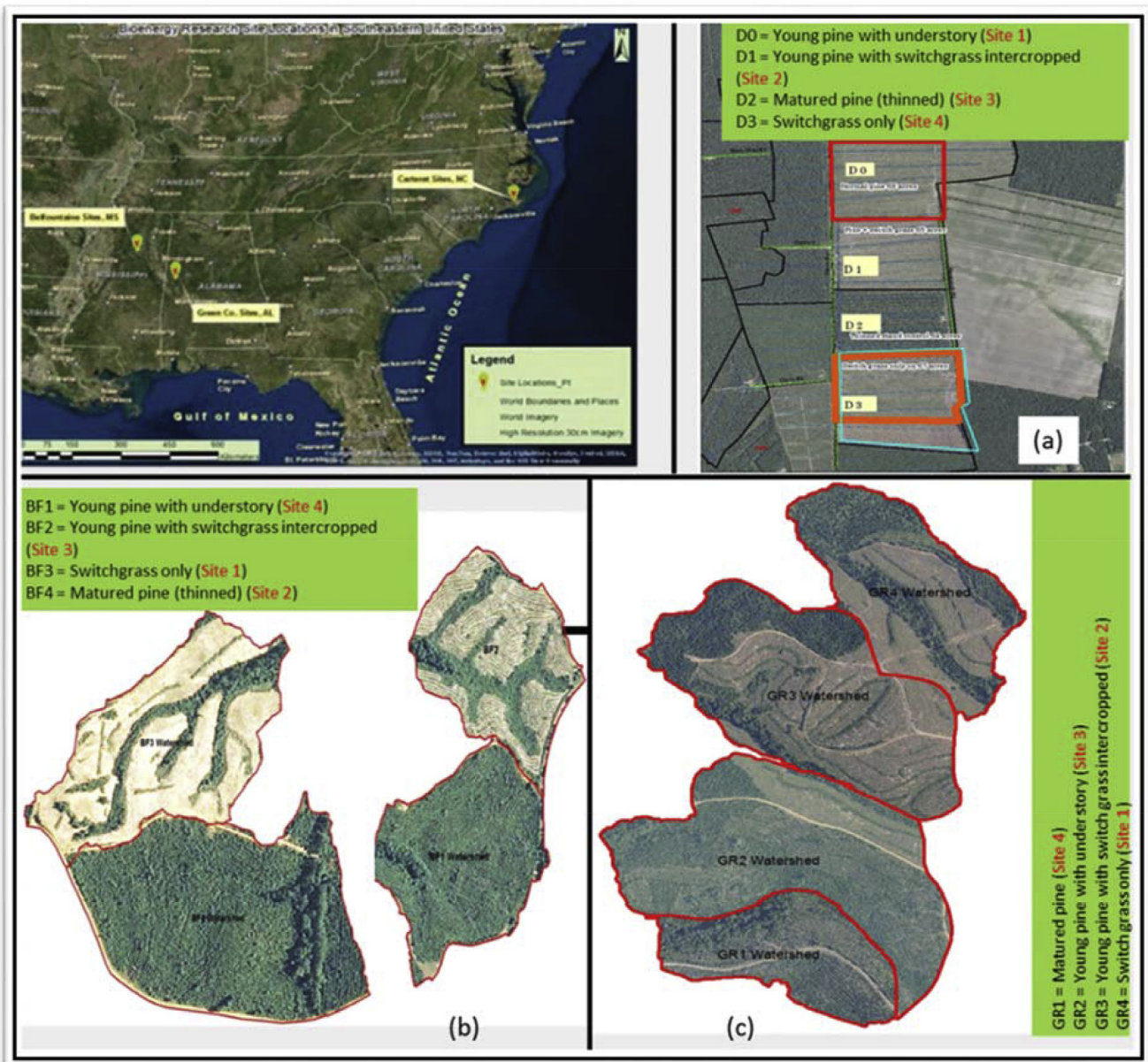


Fig. 2. Location of the study sites in the Southeastern U.S. (Satellite image of the Southeastern U.S.) and each individual watershed (a) Carteret County, NC; (b) Calhoun County, MS; and (c) Greene County, AL with their specific vegetation types.

between beds on furrows at two specific spatial locations (Fig. 4) for real-time monitoring of soil moisture. Daily weather data with field measured vegetation parameters on LAI and maximum stomatal conductance (g_s) were used to compute the PET with the Penman-Monteith (P-M) method. However, P-M PET for a standard grass reference was used for switchgrass, as there was only a limited data on its conductance. Actual ET (AET) on each treatment watershed was estimated following the method developed by Fisher et al. (2005) as shown in Equation (1).

$$AET = f * PET \quad (1)$$

Where f is a soil moisture factor and PET is daily P-M based potential evapotranspiration. The factor f , limited by soil moisture in the root zone, was calculated as SM/SM_{100} , where SM = daily average soil moisture measured at each treatment watershed, and SM_{100} = soil moisture content at 100 cm pressure head or 10 kPa, which was estimated based on soil water characteristic data. Soil moisture characteristics were derived at the North Carolina State University Soil and

Water Laboratory using undisturbed field soil core samples taken at each of the treatment watersheds during the study period. This component of AET, limited by energy component (PET), was assumed to represent only soil evaporation and vegetation transpiration. Evaporation from canopy interception was estimated separately for the mature pine stand and was assumed negligible for other treatment watersheds.

The detailed field hydro-meteorological measurements and data analysis procedures for the study site in North Carolina have been recently reported by Ssegane et al. (2017) and by Bennett et al. (2013) for the Alabama site. The Mississippi site has a similar measurement protocol as that of the AL site.

2.2.2. Field ET parameters data collection methods

Field data (LAI, g_s , T_c , and SM) were collected from 2012 to 2014, which coincided with the satellite and aerial image acquisition periods. A LiCOR-2000 instrument was used in the field for in situ LAI measurement of individual forest species such as pine (young and matured),

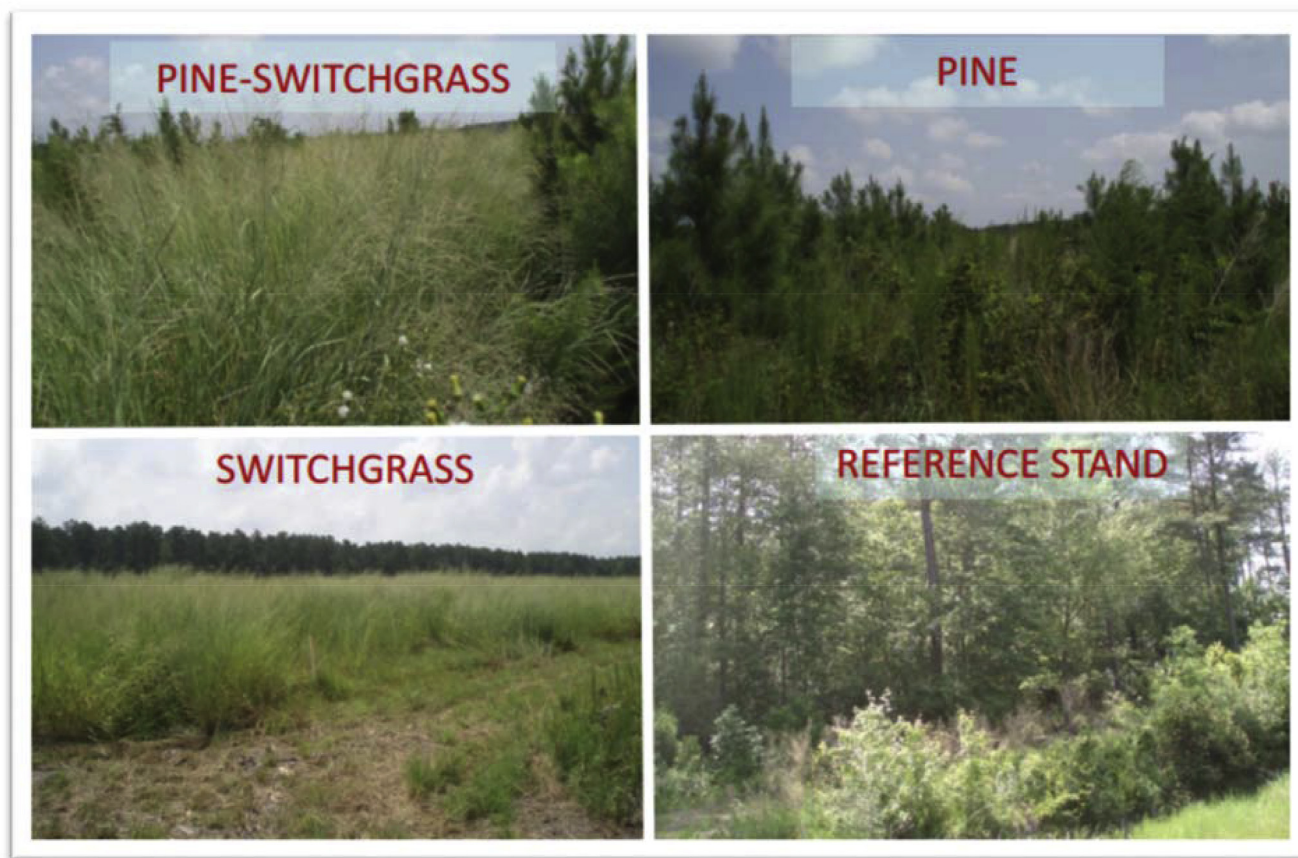


Fig. 3. Treatment vegetation examples for each of the three research sites.

switchgrass, and understories. A LiCOR-1600 porometer field instrument was used to collect g_s values for each species of vegetation. A Decagon portable volumetric water content measuring instrument was used to collect spatial soil moisture data in each watershed to supplement the soil moisture data recorded at specific locations in the watersheds as described above (Fig. 4). The air temperature measured at the site weather station was assumed as a proxy for the T_c data, as the sensor height mostly coincided with the height of young pine, switchgrass, and understories. The above field-measured data and estimated daily AET as described earlier were used as output parameters for validation of the remote sensing digital information-based ET and ET parameter estimation model development.

2.3. Image acquisition and processing

2.3.1. Image selection

Digital information from free remotely-sensed images like the Landsat 7 ETM+ and Landsat 8 (30m) along with acquired SPOT (10m) multispectral (MSS) and ultra-high resolution 4-band orthoimagery (0.15m) images were used in the study to extract spectral band information as input model parameters to estimate the ET and ET parameters for the four types of vegetation. Landsat images were chosen as the source of spectral bands for analysis as they are free, easily downloadable, and can be easily processed due to the fact that the geometric and radiometric correction (<https://earthexplorer.usgs.gov/>) has already been completed. The Landsat images have a moderate spatial resolution of 30m, and they cover the homogenous pine and switchgrass vegetation spatial area uniformly. Landsat imageries have a temporal resolution of 16 days. As both Landsat 7 ETM+ and Landsat 8 images were acquired in the same year (part of 2013 and 2014) the temporal resolution period was reduced to eight days. Thus, the ET

variation in the vegetation could be determined approximately twice monthly and in some cases four times a month, capturing seasonal variation. Landsat images have complete required spectral resolution for ET estimation – have individual bands suitable to estimate the eco-hydrologic parameters related to ET and ET parameters (Fig. 5). Landsat images also have simple radiometric resolution, i.e., 8-bit for Landsat 7 ETM+ and 16-bit for Landsat 8, which both require extra processing to make the imagery data compatible for model development.

Along with the freely available cloud-free Landsat images, SPOT images were acquired (Table 1) through Astrium Services (Richmond, VA, USA) to analyze the intercropped vegetation (young pine + understory and young pine + switchgrass). SPOT imageries were acquired at a cheaper cost when compared to other similar or slightly better, higher spatial resolution imageries. Another advantage of using the SPOT imagery was the availability of spectral bands (Fig. 5) that are suitable to estimate the eco-hydrologic parameters related to ET and ET parameters under study. The biggest advantage of using the Astrium Services images is that they radiometrically corrected the SPOT images before providing them to their users. Processed (enhancing spatial resolution to explain a 6 m spaced intercropping of pine and switchgrass/understory rows) SPOT imageries were suitable for intercropped switchgrass eco-hydrologic parameter estimation through model development. Ultra-high (0.15m) resolution orthoimages were collected for all three sites (Table 1) through Quantum Geospatial Inc. (Atlanta, Norcross, USA) to correlate with the localized ET and ET parameter (LAI and g_s) data that were collected on a transect-basis coinciding with the date of image acquisition.

2.3.2. Image processing

2.3.2.1. Geometric and radiometric correction. Geometric correction of

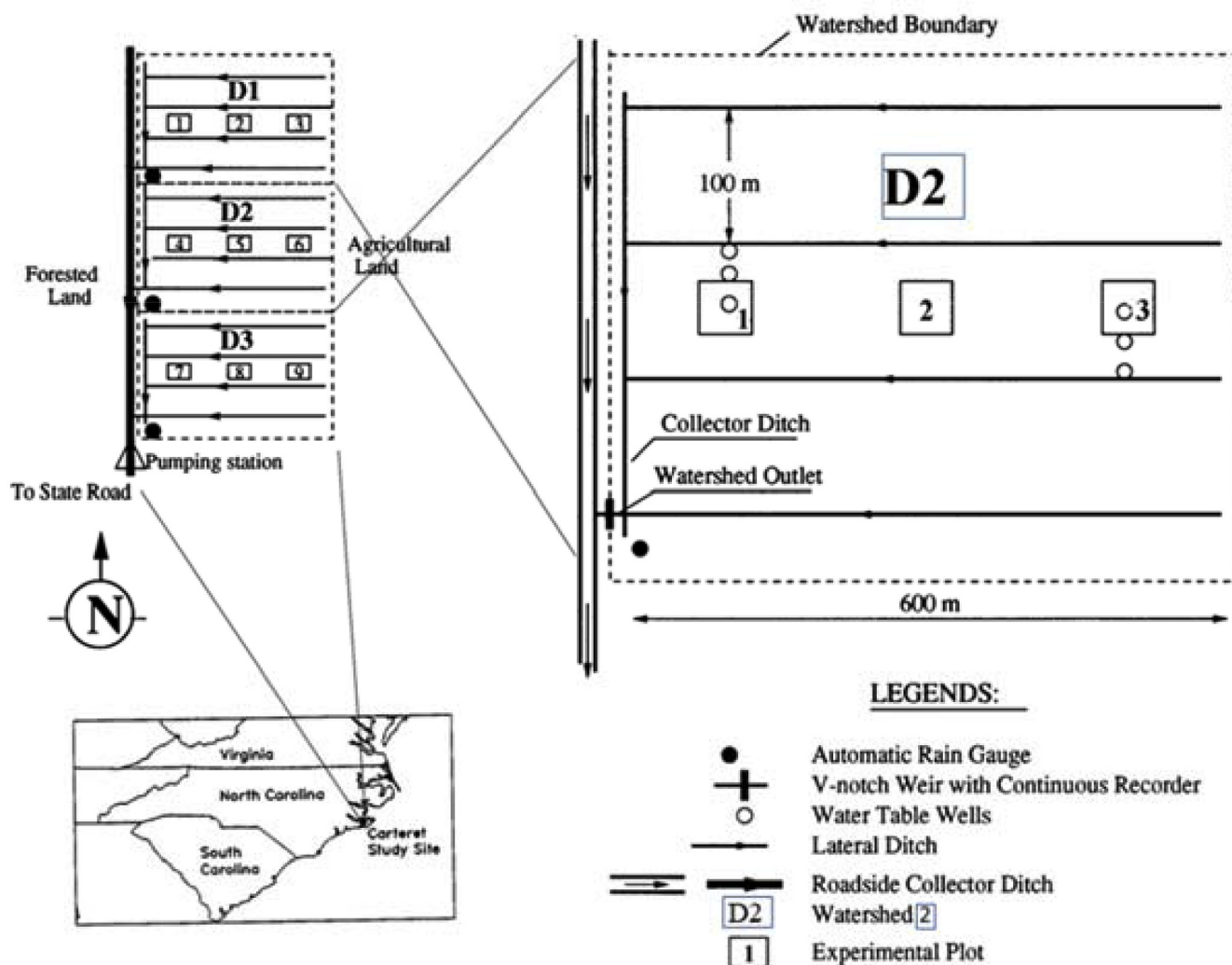


Fig. 4. Location map and experimental layout design of four treatment watersheds at Carteret, NC site – an example.

the SPOT images was completed using the Georeferencing tools available with ArcGIS 10.5 software (Redlands, CA, USA). Ground control points (GCP - road cross-sections, river bends, and some monument locations) were obtained from the referenced NAIP imageries of the study area to help in the geometric correction. However, geometrical correction of the orthoimages was completed using the GCPs set up in the field before the image acquisition. Colored plates with known reflectance values were placed in the field as ground control points with known coordinates. Colored plates image reflectance values were correlated with the actual values to develop an algorithm, which in turn was applied to the orthoimages through Raster Calculator for radiometric correction. We followed the procedure developed by Panda (2002) and Panda et al. (2010). It is to be noted that Landsat imageries were geometrically and radiometrically corrected before being disseminated to the public, and the SPOT images were acquired with completed radiometric correction.

2.3.2.2. Image fusion approach for spatial resolution set-up. SPOT MSS images have a 10m resolution while SPOT Panchromatic images have 5m resolution. ‘Pansharpening (ERDAS Imagine) with a Modified Intensity, Hue, Saturation Resolution merge’ algorithm and ‘Resample (ArcGIS 10.5)’ tools were used to have 5m resolution SPOT MSS available to us for our study. The SPOT MSS (5m) matched well to the 6-m spacing between the pine trees in the intercropped site.

Orthoimages used in the study to increase the acquired data numbers (acquisition was completed during the time different from Landsat and SPOT) were of 15 cm resolution. For ET and ET Parameter estimation modeling, they were resampled/pansharpened to 5m resolution. Resampled SPOT and orthoimages digital data were used for pine + switchgrass and pine + understory intercropped model development. This image fusion technique helped in enhancing data numbers for effective model and subsequent algorithm development in studied landuses’ ET and ET parameter estimation using remotely-sensed data.

2.3.2.3. Scanlines correction, image masking, image index development, and digital ASCII value extraction automation. Scanlines exist with Raw Landsat 7 ETM + images. Therefore, a Python script (Appendix A) was written to remove them. Scanlines are NoData values inside images. The Python script took a 15 × 15 neighborhood of pixels (specified) using the Focal Statistics tool of ArcGIS and calculated the mean value of these 225 pixels and added/inserted them in place of the NoData values of the image. The script also did the batch processing for all Landsat 7 ETM + image scanline corrections. All processed images (Landsat 7 ETM+ and 8, SPOT, and orthoimagery) were clipped to individual watersheds as the initial models were developed with the entire spatial extent for each of the watershed’s prescribed vegetation covers (Fig. 2).

Individual bands were separated from the composite image (for

Landsat 8		
Band	Band width (μm)	Environmental monitoring application
Band 1 (Coastal Aerosol)	0.43 – 0.45	coastal and aerosol studies
Band 2 (Blue)	0.45 – 0.51	Bathymetric mapping, distinguishing soil from vegetation and deciduous from coniferous vegetation
Band 3 (Green)	0.53 – 0.59	Emphasizes peak vegetation, i.e., plant vigor assessment
Band 4 (Red)	0.64 – 0.67	Vegetation slopes and plant chlorophyll content differentiation
Band 5 (Near Infrared)	0.85 – 0.88	Biomass content estimation and shorelines delineation/differentiation
Band 6 (Shortwave Infrared 1)	1.57 – 1.65	moisture content of soil and vegetation discrimination: cloud and snow differentiation
Band 7 (Shortwave Infrared 2)	2.11 – 2.29	Improved moisture content of soil and vegetation discrimination: improved cloud and snow differentiation
Band 8 (Panchromatic)	0.50 – 0.68	Higher image resolution (15 m) – sharper image definition
Band 9 (Cirrus)	1.36 – 1.38	Improved detection of cirrus cloud contamination
Band 10 (Thermal Infrared 1)	10.60 – 11.19	Lower resolution (100 m) - thermal mapping and soil moisture estimation
Band 11 (Thermal Infrared 2)	11.5 – 12.51	Lower resolution (100 m) - improved thermal mapping and soil moisture estimation

Landsat 7 ETM+ Band (μm)	Applications	SPOT 4 Band (μm)
Band 1 – Blue IR (0.45 – 0.52)	Coastal water mapping, soil/vegetation differentiation, deciduous/coniferous differentiation	Band 1 (0.50 – 0.59) (Green)
Band 2 – Green (0.52 – 0.60)	Green reflectance from healthy vegetation, iron content in rocks and soil	Band 2 (0.61 – 0.68) (Red)
Band 3 – Red (0.63 – 0.69)	Chlorophyll absorption for plant differentiation	Band 3 (0.79 – 0.89) (Near-Infrared)
Band 4 – Near IR (0.76 – 0.90)	Biomass survey, water body delineation	Band 4 (1.58 – 1.75) (Mid-Infrared)
Band 5 – Mid IR (1.55 – 1.75)	Plant moisture content, cloud/snow differentiation	
Band 6 – Thermal IR (10.4 – 12.5)	Thermal mapping, soil moisture	
Band 7 – Mid IR (2.08 – 2.35)	Soil analysis	

Color Infrared (CIR) Orthoimagery

Band 1 (0.45 – 0.53 μm) – Blue (water mapping, soil/vegetation differentiation, deciduous/evergreen forest differentiation)
Band 2 (0.53 – 0.63 μm) – Green (greenness in vegetation differentiation)
Band 3 (0.63 – 0.69 μm) – Red (chlorophyll absorption for plant differentiation)
Band 4 (0.75 – 0.90 μm) – NIR (chlorophyll absorption, biomass amount, waterbody delineation study)

Fig. 5. Image (used in this study) spectral band-based environmental (ET and ET parameters related) application descriptions (Updated from source <https://landsat.usgs.gov/what-are-best-spectral-bands-use-my-study>).

Table 1
Additional information regarding the images used in this study.

Image Type	Acquisition Dates			Resolution (m)
	Carteret, NC	Calhoun, MS	Greene, AL	
SPOT MSS	Jun 27, 2013	May 21, 2013	May 21, 2013	10m but pan-sharpened to 5m
	May 08, 2013	Oct 24, 2013	Oct 24, 2013	
	Oct 27, 2013	Jun 15, 2014	Aug 22, 2014	
	Oct 10, 2014	Sep 23, 2014	Oct 19, 2014	
	Jun 15, 2013	Sep 14, 2013	Oct 10, 2013	
CIR (4 Band) (NAIP)	Sep 12, 2013	Jun 13, 2014 (NAIP)	Jun 14, 2014 (NAIP)	0.15m
	Jun 14, 2014	Jun 19, 2014	Jun 18, 2014	
	Aug 27, 2014	Aug 28, 2014	Aug 15, 2014	
	Landsat 7	All cloud free dates (Only field data collection)		
Landsat 8	dates were used in the study. This is also applicable to SPOT and CIR images)			

SPOT and orthoimagery; Landsat bands were individually stacked when downloaded from the Earth Explorer (<https://earthexplorer.usgs.gov/>) site using the ArcCatalog band separation tool. Vegetation indices were developed using Equation (2) for the normalized difference vegetation index (NDVI), Equation (3) for the soil adjusted vegetation index (SAVI), and Equation (4) for the vegetation vigor index (VVI):

$$NDVI = (\rho_{ir} - \rho_r) / (\rho_{ir} + \rho_r) \tag{2}$$

$$SAVI = \left[\frac{\rho_{ir} - \rho_r}{\rho_{ir} + \rho_r + L} \right] \times (1 + L) \tag{3}$$

$$VVI = (\rho_{ir} - \rho_g) / (\rho_{ir} + \rho_g) \tag{4}$$

Where, ρ_r , ρ_g and ρ_{ir} are spectral reflectance from the red-, green- and NIR-band images as shown in Fig. 4, respectively, and the L is a constant that represents the vegetation density. Huete (1988) defined the optimal adjustment factor of L = 0.25 for higher vegetation density in the field, L = 0.5 for intermediate vegetation density, and L = 1 for low vegetation density. Automated geospatial models were developed in the

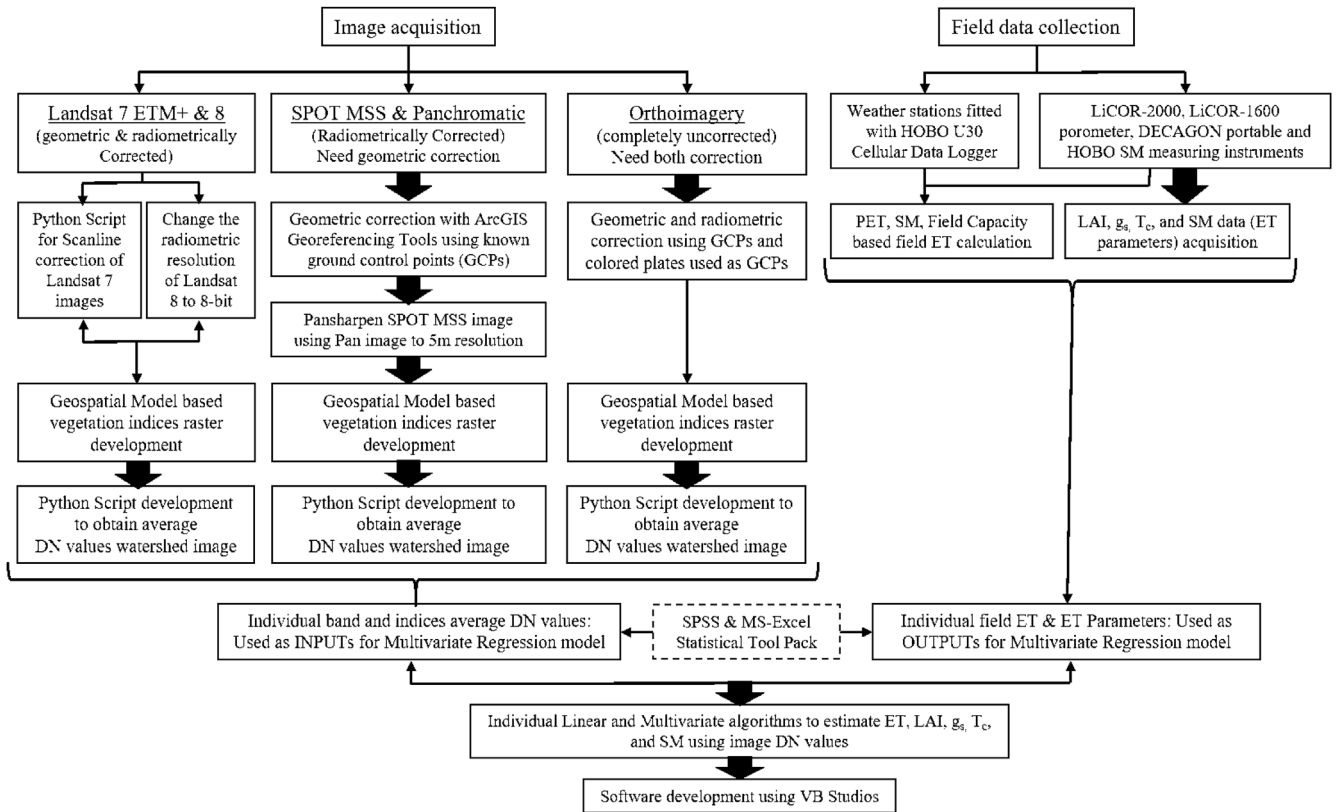


Fig. 6. Cartographic model explaining the systematic procedure of developing software to estimate ET, LAI, g_s , T_c , and SM using optical image digital number (DN) values.

ArcGIS ModelBuilder platform to automate the spectral vegetation image development. It is to be noted that image rasters in ArcGIS software are considered as Integer data type rasters and therefore, indices development (using Equations (2)–(4)) using direct raster bands would not yield correct index images (with decimal data type pixel ASCII). Therefore, during the model building in ArcGIS ModelBuilder, each of the image raster bands were converted to Float data type rasters, and the Float data type rasters were used in the Raster Calculator tool to generate the index rasters. All of the input band and index images were extracted to the watershed sizes using scripts written in Python, and the script helped in batch processing too. A Python script was written to automate and batch-process the processed images to obtain watershed average digital ASCII values through zonal statistics and use them as input parameters in the model development for estimated ET and ET parameters. Some data gaps were there due to possible field instrument malfunction during data collection, weather anomalies, and other human error in field measurements, a detailed data mining approach was followed (as shown in below subsection) to prepare appropriate data for the modeling development with statistical and ANN approaches (Panda et al., 2018).

2.4. Data mining approaches for model data preparation

Preprocessing of input data was completed with the following methods. Generally, missing values in a dataset are filled in through the use of the “attribute mean” of the dataset (Han and Kamber, 2001), most probable value (Han and Kamber, 2001), or a global constant (Han and Kamber, 2001). Though, for a few, the mean of the group was used to fill the missing numbers for our datasets. Few outliers in our datasets were observed with initial visual interpretation. However, they were ascertained by a separability function -a higher separability value suggested a great degree of distinctness in groups. The separability equation used was represented as follows:

$$V = \frac{\mu_i - \mu_j}{\sqrt{\delta_i + \delta_j}} \quad (5)$$

where, μ_i is the mean of the group i , μ_j is the mean of the group j , δ_i is the standard deviation of the data in group i , and δ_j is the standard deviation of the data in group j . Group i was the digital values obtained through image fusion and other analyses approaches described earlier, and group j included the corresponding ET and other ET parameter values. The authors did not envision any data volatility due to drastic weather changes during the three-year study because data was collected in favorable weather conditions. Testing for data integration was essential for our datasets as the imagery data were collected from four different sources (Landsat 7 ETM +, Landsat 8, SPOT, and aerial along with ET and ET parameters data with instrumentation). Thus, proper integration of these various datasets was needed in order for the data to work as a single entity, which assisted in bringing the digital data into a similar range as the Landsat 7 DN (reflectance percentage) values of 0–255 (8-bit data) and the Landsat 8 digital values of 0–65535 (16-bit data) (Panda et al., 2018). Thus, the correlation between attributes A (image data) and B (ET and ET parameters data) was obtained by the following formulae:

$$r_{A,B} = \frac{\sum (A - \bar{A})(B - \bar{B})}{(n - 1)\sigma_A\sigma_B} \quad (6)$$

where, n is the number of data points, A and B are means of two different attribute values, and σ_A and σ_B are standard deviations of the respective attribute values. When the value of $r_{A,B}$ was greater than 0 and A and B were positively correlated, the formula resulted in a high value, and thus implied redundancy in the attributes. We also completed data transformation for our study due to data volatility as described above. Therefore, to enable the dataset to be ANN model friendly, data normalization was completed with our dataset to bring the image digital values and ET and ET parameter values into similar

ranges. In the neural networks literatures, data normalizing also often refers to rescaling the vector by the minimum and the range to make all elements lie between 0 and 1. Panda et al. (2018) explained in their study that data normalization is generally completed by subtracting a measure of location and dividing by a measure of scale; e.g., if the vector contains random values with a Gaussian distribution, subtract the mean and divide by the standard deviation to obtain a “standard normal” variable with a mean of 0 and a standard deviation of 1 (Equation (3)).

$$X_N = \frac{X_i - \mu}{\delta}, \tag{7}$$

where, N is the number of training cases; X_i is the value of the raw input variable, X , for the i th training case; X_N is the normalized value of X ; μ is the mean of data points; and δ is the standard deviation of data points. After data outliers were determined and data volatility reduction with normalization was conducted, new datasets were created for both statistical and neural network model development. The entire work process is shown as a cartographic model in Fig. 6.

2.4.1. ET and ET parameter estimation model development

2.4.1.1. *Statistical modeling approach.* The ASCII format of data from developed NDVI, SAVI, and VVI were used as input parameters for the LAI (output) multivariate model development. The g_s linear regression model was developed using the Band 4 (SPOT), Band 5 (Landsat 7 ETM+), and Band 6 (Landsat 8) digital image information. Band 6 (Landsat 7 ETM+) and Band 10 (Landsat 8) digital image information were used for the canopy temperature estimation model development. Band 7 (Landsat 7 ETM+) and Band 7 (Landsat 8) were used for the development of SM remote estimation model. Table 2 shows the detailed, image-based parameters combination (as input parameters) for the ET and ET parameter estimation multivariate model development. Initial ET estimation modeling was carried out using all of the digital image information discussed above.

Simple regression analyses were conducted for the models using a single image factor ASCII value. The analyses were completed using the MS-Excel Statistical Tool Pack. The best-fit trend line curves were developed along with the provision for the correlation algorithm (equation) and the coefficient of determination (R^2) value for the best-fit models. As described in Table 2, initially all image-based parameters were used as input parameters for ET estimation model development for each watershed (different vegetation covers). Backward step-wise regression was used to obtain the best model input combination for each of the different watershed vegetation covers, as there were a small number of variables to work with. Multicollinearity tests of the input parameters were completed separately for ET estimation model development. The analysis explained that red and NIR (near infrared) bands are very similar and VVI is similar to NDVI, which was supported by step-wise regression modeling. It should be noted that all of the digital image information and ET and ET parameter multivariate models were developed in the MS-Excel Statistical Tool Pack's multivariate regression analysis tool using the appropriate parameters established through the multicollinearity analysis and step-wise regression. For the LAI estimation models, all three vegetation indices were used as input

parameters to develop multiple regression models. The p-value statistics were used to test the null hypothesis that the coefficient is equal to zero (no effect). With low p-value (< 0.05), it was understood that a predictor was meaningful to our models because changes in the predictor's value are related to changes in the response variable. The model regression coefficients represent the mean change in the response variable for one unit of change in the predictor variable while holding other predictors as constant, which is important in the analyses, as it isolates the role of one variable from all of the others. Using regression coefficients, we were able to develop the ET parameters and ET prediction algorithms that were useful in software development to predict ET parameters and ET with appropriate remotely-sensed digital information.

When feasible (when more data points were available), the models that were developed with the 2012 and 2014 data were validated with the data from 2013. In some cases, the model validations were completed with an extra mix of data from other years, as enough data was not available from 2013. Average Absolute Prediction Accuracy (AAPA) was computed for the validation models using Equation (5).

$$AAPA (\%) = \left(\frac{1}{n} \sum_1^n (Abs(Actual - Predicted))/Actual \right) * 100 \tag{8}$$

where, n = number of observations.

2.5. Artificial neural network modeling approach

Artificial neural network (ANN) modeling techniques were adapted to enhance the remote estimation of ET in pine, switchgrass, pine-switchgrass intercropping, and pine-understory intercropping vegetation, as statistical models for such ET estimation proved to be inferior. The RBFN modeling approach was used to develop such models.

A typical RBFN consists of three different layers with successive layers fully connected by feed-forward arcs, as shown in the RBFN model architecture pertaining to our research and in Fig. 7. There is no provision of weight between the input layer and the hidden layer (prototype) while a nonlinear transfer function (i.e., radial basis function) is used at the hidden layer (Fig. 7). This study presents two input parameters (Landsat PC1 and 2 band digital information) in the input layer, as opposed to the RBFN model, which includes just one hidden layer. Generally, in the RBFN model, the output layer is linear (Haykin, 1999) but in this study, the RBFN model was nonlinear due to the application of the Gaussian transfer function in the network.

A step-by-step model optimization procedure was developed for this study, following the procedural flow chart shown in Panda et al. (2010), to obtain the best correlation between input and output parameters in RBFN. The learning rate, momentum term, and iteration rates were changed alternately to optimize the RBFN models so that optimal prediction accuracies were obtained. The datasets for individual landuse based ET and ET parameters models were divided as a training and testing dataset with a random 70–30 percent ratio, where feasible, as in a few cases less than five data points available. First, the models were optimally trained, then the testing data was used in both models to validate the optimal training model's estimation efficacy as discussed

Table 2
Image spectral band and index combination of Landsat, SPOT, and orthoimagery to estimate ET and ET parameters.

Image band and index combination as model input parameters				Model output parameters
Landsat 7 ETM+	Landsat 8	SPOT	Orthoimagery	
Band 8 (TIR)	Band 10 (TIR-1)			Canopy temperature
Band 5 (MIR-1)	Band 6 (SWIR-1)	Band 4 (MIR)		Stomatal conductance
NDVI, SAVI, VVI	NDVI, SAVI, VVI	NDVI, SAVI, VVI	NDVI, SAVI, VVI	Leaf area Index
Band 7 (MIR-2)	Band 7 (SWIR-2)			Soil moisture
All of the above	All of the above	All of the above	All of the above	Evapotranspiration (ET)

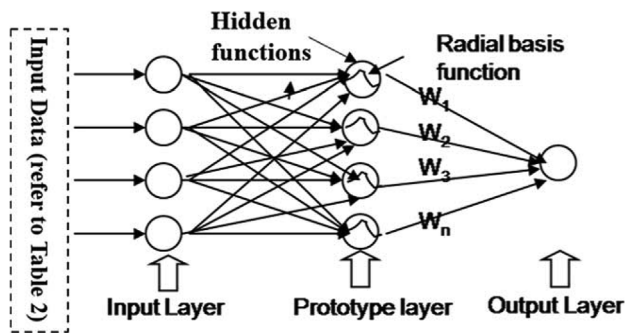


Fig. 7. The RBFN model architectures developed for estimation of ET, LAI, canopy temperature, stomatal conductance, and soil moisture for each landuse type (pine, switchgrass, pine and switchgrass intermix, and pine and understory intermix).

below, also known as the RBFN model evaluation process.

The RBFN model performances were evaluated based on root mean square error (RMSE), prediction accuracy, and standard error of prediction (SEP). Moreover, the correlation coefficient (r) between the actual and predicted output along with the slope and intercept of the linear regression model was used in model performance evaluations. The equation for RMSE is:

$$RMSE = \sqrt{MSE} = \sqrt{\frac{SSE}{n-p}} \quad (9)$$

where, n is the number of observations; p is the number of the parameter to be estimated; and SSE and MSE are sum of squared errors and mean square error, respectively.

Average test prediction accuracy is calculated based on Equation (10), where N is the total number of observations and OP_A and OP_P are actual and predicted output, respectively.

$$\text{Average Test Accuracy} = \left(1 - \frac{1}{N} \sum_{i=1}^N \frac{|OP_A - OP_P|}{OP_A} \right) \times 100 \quad (10)$$

An executable file developed in the Biolab of North Dakota State University, Fargo ND, using Visual C++ (Microsoft Corporation, Bellevue, WA) was used to determine the predicted ET accuracy and the subsequent actual and predicted correlation coefficient (r) between the measured and predicted ET and, intercept (a), slope (β), and SEP from the back-propagation neural network result. The predicted and actual output regression analysis was completed using the following linear equation:

$$Y = \beta X + a \quad (11)$$

Where, X and Y are predicted and actual output, respectively; β is slope; and a is the intercept. The SEP of the predictive model is calculated by using the following equation by Kramer et al. (2001):

$$\sqrt{\frac{\sum_{i=1}^n [(Y_i - X_i) - d_m]^2}{n-1}} \quad (12)$$

where, d_m is the mean of the difference between actual and predicted values Y and X (of i th individual), respectively; and n is the total number of observations.

2.5.1. Software development

The relationship between input and output data, i.e., the statistical multiple regression correlation algorithms, were used to develop executable files (software) in the object-oriented programming language Visual Basics Studios (Microsoft, Bellevue, WA). The executable files were created as forms so that they can be used by laypersons to estimate the pine, pine + switchgrass intercropped vegetation, switchgrass, and pine + natural understory vegetation ET and ET parameters from

Table 3

Multicollinearity matrix obtained from the digital image parameters used in the study (an example).

Bands	B5	B6	B7	NDVI	SAVI	VVI
B5	1					
B6	0.23	1				
B7	0.29	-0.10	1			
NDVI	-0.04	0.05	-0.15	1		
SAVI	0.04	0.05	-0.11	0.96	1	
VVI	0.30	0.39	-0.34	0.42	0.42	1

image digital information by entering the input values in to designated text boxes and clicking on the CALCULATE button.

3. Results and discussion

3.1. Multicollinearity analysis on image bands for model development

When one predictor variable in a multiple regression model can be linearly predicted from the others with a substantial degree of accuracy, it creates a situation, where the coefficient estimates may change erratically in response to small changes in the model or the data is the multicollinearity phenomenon (Pottel, 2003). Pottel (94), in his study on 'Problems of using Microsoft Excel for statistics,' mentioned the advantage of performing multicollinearity analysis before performing multivariate regression. The LAI and ET estimation models used multiple digital image parameters as explanatory variables. Therefore, to ascertain the efficiency of each parameter in model development, multicollinearity analyses were completed in MS-Excel statistical Tool Pack software. Results of a multicollinear analysis in Table 3 revealed that SAVI and NDVI are essential pieces of information, although similar, for the model building in this study and have 96 percent collinearity. Therefore, we have alternately used the information SAVI and NDVI in model development. VVI image information has some degree of multicollinearity (coefficient of 0.42) with both NDVI and SAVI. Multicollinearity analysis helped us determine the best bands to use in multivariate model development for LAI and ET estimation model development (Table 4).

3.2. Image information-based ET and ET parameter (LAI, g_s , T_c , and SM) models

3.2.1. Switchgrass only

For remote estimation of the switchgrass (only) ET parameters, model development that uses Landsat, SPOT, and orthoimagery digital information with an acceptable coefficient of determination (LAI: $R^2 = 0.77$, $n = 14$; g_s : $R^2 = 0.70$, $n = 18$; T_c : $R^2 = 0.77$, $n = 34$; and SM: $R^2 = 0.68$, $n = 12$) were obtained. Average prediction accuracies of 70.05, 94.88, 89.93, and 90.61 percent were obtained with the g_s , T_c , SM, and LAI models, respectively (Table 4). The model result is based on the analyses of the validation dataset. The model data were randomly separated as training data and testing data. Once the multivariate regression models were developed, the algorithm (using the input parameter coefficient and intercept coefficient) for ET or ET parameter estimation was developed and the same algorithm was used to estimate the ET or ET parameter values. A correlation analysis was created using the actual field data and the model-based predicted data as the results of the validation model data. The low correlation among the actual field data and the model-based predicted data could be attributed to the inconsistent growth of switchgrass in the homogenous research plots and in the research plots where it was grown as an intercrop with young pine during the study period (2012–2014). The multivariate ET estimation model provided $R^2 = 0.50$, standard error of prediction (SEP) = 0.94 (18 percent of the observed ET average), and an average prediction accuracy of 82.09 percent with $n = 55$ for the

Table 4
RBFN Model architecture, optimized parameters, and modeling validation results for estimating ET and ET parameters.

Vegetation type	ET & ET parameter	RBFN Model architecture & modeling parameter					Testing model validation results						
		'Input – Hidden – Output' neurons	Learning rate	Moment-um term	Epochs	Learning rule	Transfer function	RMSE	Classification rate (%)	Data cor-relation rate	Average accuracy (%)	r	SEP (%)
Switchgrass	ET	5-3-1	0.5	0.9	40,000	Delta-Rule	Sigmoid	0.004	1	0.9	85	0.76	15.1
	g _s	Linear model with one input	0.6	0.8	50,000	algorithm	Function	0.005		0.85	84	0.77	17.2
	T _c	Linear model with one input	0.6	0.9	50,000			0.0018		0.99	92	0.88	11.5
	LAI	3-2-1	0.5	0.9	50,000			0.0048		0.85	81	0.71	18.2
Pine + Switchgrass	SM	Linear model with one input	0.5	0.8	80,000			0.47		0.45	55	0.54	27.3
	ET	5-2-1	0.5	0.9	50,000			0.021		0.84	75	0.71	18.3
	g _s	Linear model with one input	0.5	0.9	50,000			0.013		0.81	74	0.69	19.8
	T _c	Linear model with one input	0.5	0.9	50,000			0.007		0.91	86	0.86	14.5
	LAI	3-2-1	0.5	0.9	50,000			0.05		0.65	73	0.69	21.2
	SM	Linear model with one input	0.5	0.9	50,000			0.08		0.38	46	0.51	35.8
Pine + Understorey	ET	5-2-1	0.5	0.9	50,000			0.04		0.92	76	0.73	18.7
	g _s	Linear model with one input	0.5	0.9	50,000			0.05		0.75	81	0.69	22.3
	T _c	Linear model with one input	0.5	0.9	50,000			0.016		0.89	90	0.81	16.6
	LAI	3-2-1	0.5	0.9	50,000			0.055		0.75	61	0.68	24.0
	SM	No data											

estimation of ET in switchgrass (only) plots. The relatively poor performance could be attributed to the inconsistent spatial and temporal growth of switchgrass in those plots.

3.2.2. Switchgrass intercropped with pine

Remotely-sensed image information (that uses Landsat, SPOT, and orthoimagery digital information) for pine and switchgrass intercropped pine forest ET parameter estimation models provided somewhat inferior model input-output correlation, i.e., coefficient of determination (LAI: $R^2 = 0.59$, $n = 24$; g_s : $R^2 = 0.56$, $n = 22$; T_c : $R^2 = 0.81$, $n = 36$; and SM: $R^2 = 0.10$, $n = 4$) values. Soil moisture remote estimation could not draw any statistical conclusion due to very small the sample size of only four. Average prediction accuracies of 54.55, 85.28, 70.64, and 88.07 percent were obtained with the g_s , T_c , and LAI models, respectively (Table 4). However, a multivariate regression analysis to estimate the soil moisture amount in pine and switchgrass intercropping plots was completed using Red, NIR, NDVI, and SAVI digital information instead of the natural Band 7 (Landsat 7 ETM+) and Band 11 (Landsat 8), which yielded a significant improvement in SM estimation accuracy (with an increase of R^2 from 0.10 to 0.57). The ET estimation model for switchgrass intercropping provided an R^2 of 0.47, standard error of prediction (SEP) = 0.99 (19 percent of observed ET average) and an average prediction accuracy of 81.44 percent with $n = 20$ when using Red, NIR, and NDVI image information as input parameters. The low correlation between the image input information and the ET and ET parameter values (field-measured data) is due to the introduction of Landsat image information to the model along with SPOT and orthoimages. The pixel size (30 m) of the Landsat data and the field row spacing of the pine and switchgrass intercropping (6m) did not match for intercropping. SPOT MSS images pan-sharpened to 5m using the panchromatic image were useful to clearly differentiate the switchgrass row vegetation from the pine vegetation along with the orthoimagery spatial resolution (15 cm). Therefore, Landsat data should not be used in the model, although, it would decrease the number of input image variables in the study. However, we have included Landsat based image information in the study, thus obtained reduced model correlation. Furthermore, it was concluded that Landsat data should not be included in the switchgrass ET or ET parameter estimation in an intercropping perspective, as the spacing of 6m is much lower than the 30m spatial resolution of Landsat.

3.2.3. Pine and understory intercropping

Pine and understory (intercropped) ET parameter remote estimation models (that use Landsat, SPOT, and orthoimagery digital information) provided poor input-output correlation with coefficients of determination values of i) LAI: $R^2 = 0.28$, $n = 27$; ii) g_s : $R^2 = 0.63$, $n = 26$; and iii) T_c : $R^2 = 0.76$, $n = 45$. There was no soil moisture model developed for pine and understory intercropping. The poor model correlation is attributed to the same factors previously discussed regarding switchgrass intercropped with pine. The ET estimation model developed for the young pine with natural understory watersheds provided an R^2 of 0.48 and an average prediction accuracy of 81.41 percent with $n = 17$ using Red, NIR, NDVI, and SAVI image information as input parameters. The multivariate model underpredicted in the majority of cases and 17 data points. The low coefficient of determination obtained with this model for estimating ET could be attributed to the heterogeneity of understory forest shrub species present in all pine with understory intercropping watersheds. Average prediction accuracy of ET parameters exceeded 80 percent, except for the g_s and SM (Table 4).

In this study, the authors did not develop any ET and ET parameter estimation models for plots containing matured pine only. However, in another companion study, the main authors of this study (15) have developed remote sensing based ET and ET parameter estimation models for plots containing matured pine only and have obtained significant input-output correlations (g_s : $R^2 = 0.61$, $n = 37$; T_c : $R^2 = 0.89$, $n = 55$; SM: $R^2 = 0.33$, $n = 39$; and ET: $R^2 = 0.61$, $n = 35$). The

authors attributed this to the homogeneity of the vegetation cover and the ability of the Landsat (30 m) images to comprehend the vegetation characteristics. However, in the intercropped sites, the ET parameter estimation input-output correlations obtained were relatively satisfactory, suggesting that remotely-sensed digital information seems like a cost-effective and efficient way of estimating ET parameters for larger spatial coverage quickly.

Through the ET and ET parameter models, the authors address the methodological question of whether remotely-sensed spectral bands can be useful for modeling evapotranspiration and its components for young pine with a recruited understory, switchgrass, and its intercropping between young pine beds. The authors have concluded that for homogenous vegetation, except the SM parameters, all other ET parameters discussed in this study and ET itself can be estimated with algorithms developed using freely available medium-resolution Landsat images. For intercropping vegetation, high-resolution images are required.

3.3. RBFN models

As discussed in the 'Artificial Neural Network modeling approach' section of the manuscript, proper 'Training' and 'Testing/Validation' datasets were created for the RBFN model development. The model parameters were set to optimum levels following the neural network optimization step-by-step approach. In most modeling cases, a learning coefficient of 0.5, a momentum term of 0.9, and 50,000 epochs were found to be optimum for the RBFN model architectures, along with the learning rule of the Delta-Rule algorithm and transfer function of sigmoid. With few model optimizations completed, the authors concluded that a learning coefficient of 0.5, a momentum term of 0.9, and epochs of 50,000, the learning rule of Delta-Rule algorithm, and a transfer function of sigmoid are optimal for this study's RBFN model development, and thus used them for all of the models. Table 4 details the RBFN model architecture and its optimal functionality used while modeling, along with model training and testing validation results for each landuses ET and ET parameter prediction.

Table 4 contains the training and testing RMSE, data correlation rate, actual versus desired classification rate value, model prediction testing absolute error, average accuracy, and testing models' actual versus predicted correlation coefficient (r), and SEP values. It was observed from the results, with RBFN modeling, pine and switchgrass only ET, canopy temperature, LAI, and stomatal conductance could be estimated/predicted well using the remotely-sensed image information, obviously with proper data mining (Table 4). More than 80 percent average testing model-based prediction accuracies were obtained in those cases. However, the intermix landuses provided somewhat poorer testing prediction accuracies, ranging from 60 to 80 percent. The soil moisture prediction models, like the statistical models, did not provide any remarkable results, attributed to the litter cover in the study area and the difficulty of satellite/aerial platform-based sensor data collection through the dense canopy in pine and pine intermix landuse sites. It was also concluded that more data inclusion in a few of the models might enhance their ability to predict ET and its parameters. This procedure was developed as an alternative to the less complex, simple, and user-friendly automated geospatial model and statistical model result supported executable file development approach to estimate ET and its related parameters using remote sensing digital information, as shown below. However, the ANN model is not simple for lay-users, but forest managers with access to neural network software would likely be able to apply them for ET and ET parameter estimation from described landuses by using remotely-sensed data.

3.4. Software development

Table 5 represents the multivariate model algorithms obtained to estimate ET and ET parameters for various vegetation (treatment)

Table 5

Various multivariate model algorithms obtained from the study to develop software for ET and ET parameter estimation from digital image information.

Veg. Type	ET/ET Parameter Estimation Model Algorithm	AAPA (%)	
Switchgrass	ET =	3.78 + (0.01*G)-(0.04*R) + (0.02*NIR) + (1.20*NDVI)-(2.18*SAVI)	82.09
	g _s =	$-4e^{-0.05 \cdot \text{MIR1}/\text{SWIR1}} + 0.0064$	70.05
	T _c =	(0.25*TIR Band) - 6.278	94.88
	SM =	(0.0064*SWIR2/MIR2) + 0.14	89.93
	LAI =	1.45 + (1.07*NDVI) + (1.71*SAVI) + (0.77*VVI)	90.61
Switchgrass + Pine	ET =	0.49 + (0.01*R) + (0.01*NIR)-(48.75*NDVI) + (30.16*SAVI)	81.44
	g _s =	$-4e^{-0.05 \cdot \text{MIR1}/\text{SWIR1}} + 0.0059$	54.55
	T _c =	(0.33*TIR Band) - 18.81	85.28
	SM =	(0.04*TIR Band) + 13.04	70.64
	LAI =	1.73-(0.32*NDVI)-(0.79*SAVI) + (3.55*VVI)	88.07
Pine + Understory	ET =	-0.55 + (0.04*R) + (0.03*NIR)-(1.92*NDVI)-(5.13*SAVI)	81.41
	g _s =	0.0001*MIR1/SWIR1 + 0.0078	47.45
	T _c =	(0.25*TIR Band) - 8.1	88.77
	SM =	No Data	-
	LAI =	3.67-(0.67*NDVI)-(0.03*SAVI)-(1.17*VVI)	81.26

scenarios. The equations (algorithm) in Table 5 were used to develop executable files (software) to estimate daily ET, LAI, g_s, T_c, and SM parameters using the proper digital information. The software will be available for public use as required in the GitHub site (<https://github.com/drsudhanshpanda/Software>).

3.5. Uncertainty and limitations

In this study, use of daily ET values for the watershed sites were obtained using an approximate method that used PET, SM, and field capacity as explained above, unlike other similar studies (15, 50) that compared the remote imagery-based ET with more accurate, directly measured ET by eddy covariance based methods. This may have introduced some errors. Some other uncertainties might have arisen from the measurement of field ET parameter data (LAI, and g_s including their estimates as watershed average from sample measurements), which was acquired at approximately noon (Amatya et al., 2016), in an attempt to coincide with the satellite or aerial image acquisition period. Sometimes there was a lag of as many as 2–3 days because of the field weather conditions. Authors, in their laboratory, conducted radiometric corrections for orthoimages, whereas NASA completed corrections for the Landsat images in-house, and Astrium Services Inc., completed corrections for the SPOT images with their own system. This may have also introduced some errors. The vegetation growth in the watersheds, especially the switchgrass growth, was uneven over the three years of research (2012–2014). Switchgrass plots had sporadic coverage and therefore the image pixels were essentially mixed pixels (mixels) (switchgrass and bare soil). As described previously, Landsat images (30m resolution) could not discern the vegetation in the intercropped plots. Therefore, tools (statistical models, automated geospatial models, and executable files) may not be able to predict the daily average ET and ET parameters for various types of vegetation accurately. However, we attempted to produce estimations for ET and ET parameter values from remotely-sensed image based digital information by combining different resolution images from three differing sites with topographic, climate, and environmental conditions. It is likely that some errors were introduced due to the use of specific-only bands in the analysis, as well as our use of image processing software, and instrumentation in the field.

4. Summary and conclusions

Intercropping switchgrass between tree-rows in young pine plantations can increase bioenergy feedstock production without land opportunity costs. However, intercropping could have ecological consequences, including altered water budgets due to the different ET rates

from different forest crops. Measurement of evapotranspiration (ET), a significant component of any forest water budget, across cropping systems is costly and time-consuming, so techniques for estimating ET and its parameters from remotely-sensed spectral bands could facilitate the assessment of relative ET demands among competing forest land uses. Field and corresponding image data of various spatial and spectral resolutions were used within three environmentally diverse sites over a period of three years (2012–2014) to create robust multivariate models. The models were trained with years 2012 and 2014, and validated (tested) with year 2013 data wherever feasible (if enough data samples were available). If enough data was not available, the validation or testing data were picked randomly from the full dataset to ascertain the model efficiencies (as shown in the results section). It was observed from the study that canopy temperature of any vegetation could be accurately estimated with the TIR bands of the images, which is consistent with previous studies. Stomatal conductance and LAI values, even for the complex intercropped sites, could be estimated with moderate accuracy using appropriate digital information. Evapotranspiration of switchgrass and its intercropping with pine could be reasonably well estimated using Green, Red, and NIR band digital information along with NDVI and SAVI data. The software developed using the obtained algorithm would help lay-users to approximately estimate these ecohydrologic parameters of pine, switchgrass, and intercropping for appropriate management decisions in plantation forests with ease. Our study findings suggest that when more spatial variability, sound data mining, ultra-high resolution imagery and advanced image processing approaches are included to account for potential modeling uncertainties, they will enhance these environmental parameters' remote estimation accuracy. That said, future studies using these remote sensing-based ET models should be further tested at multiple sites for quantifying the water use from switchgrass and other similar cellulosic biofuels intercropped in pine forests separately by each vegetation and/or in combination, as a part of the regional water balance and resource assessment. RBFN based models provided promising results for estimating ET and ET parameters using remotely-sensed digital information prepared with data mining. But it is assessed that lay-persons may find it difficult to use. However, forest managers with access to neural network software can use our devised RBFN training models for estimating those forest hydrologic parameters with better accuracy.

Acknowledgments

The authors would like to express their sincere thanks to the United States Department of Energy for grant support of this study. We acknowledge the support of numerous field crews, Weyerhaeuser

personnel, and undergraduate student assistants to complete the field-work and supporting in the image analyses. We also sincerely acknowledge Dr. Jami E Nettles at Weyerhaeuser Company for her great

support at various levels for completing this study and Dr. Rhett Jackson at University of Georgia for support with some field data analysis for groundtruthing at MS and AL study sites.

Appendix B. Supplementary data

Supplementary data to this article can be found online at <https://doi.org/10.1016/j.envsoft.2019.07.012>.

Appendix A. Python code for Landsat 7 scanline correction

```
import sys, os, arcpy
from arcpy.sa import *
arcpy.CheckOutExtension("Spatial")
arcpy.env.overwriteOutput = True

wd = raw_input('In which directory are your image files located?')
satellite = raw_input('With which Landsat Satellite was your imagery acquired? (5,7,8)')
date = raw_input('Was your image collected before of after May 31, 2003? (before/after)').lower()

arcpy.env.workspace = wd
raster_list=arcpy.ListRasters("", "tif")

if satellite == '7' and date == 'after':
    os.chdir(wd)
    os.makedirs('SC_Corr')
    for Ras in raster_list:
        arcpy.AddMessage("Processing" + Ras)
        desc = arcpy.Describe(Ras)
        if desc.bandCount == 1:
            arcpy.SetRasterProperties_management(Ras, nodata="1 0")
            Con(IsNull(Ras), FocalStatistics(Ras,
            NbrRectangle(15,15,"CELL"),"MEAN"),Ras).save(wd + '\SC_Corr\CORR_{}'.format(Ras))
            cd = wd + "\SC_Corr"
            arcpy.env.workspace = cd
            corr_list=arcpy.ListRasters("", "tif")
            comp_images = [raster for raster in corr_list[0:5]]
            comp_images.append(corr_list[7])

elif satellite == '7' and date == 'before':
    comp_images = [raster for raster in raster_list[0:5]]
    comp_images.append(raster_list[7])

elif satellite == '8':
    comp_images= [raster_list[0]]
    comp_images += raster_list[3:10]

elif satellite == '5':
    comp_images = [raster for raster in raster_list[0:5]]
    comp_images.append(raster_list[6])

arcpy.CompositeBands_management(comp_images, "Final_Composite.tif")
```

References

- Albaugh, J.M., Domec, J.-C., Maier, C.A., Sucre, E.B., Leggett, Z.H., King, J.S., 2014. Gas exchange and stand-level estimates of water use and gross primary productivity in an experimental pine and switchgrass intercrop forestry system on the Lower Coastal Plain of North Carolina. *U.S.A. Agricultural and Forest Meteorology* 192–193, 27–40.
- Amatya, D.M., Harrison, C.A., 2016. Comparison of potential evapotranspiration (PET) using five methods for a grass reference and a natural forest in coastal plain of South Carolina. *J. Hydrol. Eng.* 21 (5), 1–13.
- Amatya, D.M., Skaggs, R.W., 2001. Hydrologic modeling of pine plantations on poorly drained soils. *For. Sci.* 47 (1), 103–114.
- Amatya, D.M., Skaggs, R.W., 2011. Long-term hydrology and water quality of a drained pine plantation in North Carolina. *Trans. ASABE (Am. Soc. Agric. Biol. Eng.)* 54 (6), 2087–2098.
- Amatya, D.M., Skaggs, R.W., Gregory, J.D., 1996. Effects of controlled drainage on the hydrology of a drained pine plantation in the North Carolina Coastal Plains. *J. Hydrol. (Amst.)* 181 (1–4), 211–232.
- Amatya, D.M., Gilliam, J.W., Skaggs, R.W., Lebo, M.E., Campbell, R.G., 1998. Effects of controlled drainage on forest water quality. *J. Environ. Qual.* 27 (4), 923–935. <https://doi.org/10.2134/jeq1998.00472425002700040029x>.
- Amatya, D.M., Irmak, S., Gowda, P., Sun, G., Nettles, J.E., Douglas-Mankin, K.R., 2016. Ecosystem evapotranspiration: challenges in measurements, estimates, and modeling. *ET Special Collection. Trans. of the ASABE.* 59 (2), 555–560.
- Bastiaanssen, W.G.M., Menenti, M., Feddes, R.A., Holtslag, A.A.M., 1998. A remote sensing surface energy balance algorithm for land (SEBAL). 1. Formulation. *J. Hydrol.*

- 212, 198–212.
- Beltran, B.J., Amatya, D.M., Youssef, M., Jones, M., Callahan, T.J., Skaggs, R.W., Nettles, J.E., 2010. Impacts of fertilization on water quality of a drained pine plantation: a worst case scenario. *J. Environ. Qual.* 39, 293–303. <https://doi.org/10.2134/jeq2008.0506>.
- Bennett, E.R., 2013. Hydrology and Water Quality Impacts of Site Preparation for Loblolly Pine (*Pinus taeda*) and Switchgrass (*Panicum virgatum*) Intercropping in Upland Forested Watersheds in Alabama. M.S. Thesis. N. C. State University, pp. 280p.
- Brauman, K.A., Freyberg, D.L., Daily, G.C., 2012. Potential evapotranspiration from forest and pasture in the tropics: a Case study in Kona, Hawaii. *J. Hydrol.* 440–441, 52–61.
- Cammalleri, C., Anderson, M.C., Gao, F., Hain, C.R., Kustas, W.P., 2013. A data fusion approach for mapping daily evapotranspiration at field scale. *Water Resour. Res.* 49 (8), 4672–4686. <https://doi.org/10.1002/wrcr.20349>.
- Carter, G.A., 1998. Reflectance wavebands and indices for remote estimation of photosynthesis and stomatal conductance in pine canopies. *Remote Sens. Environ.* 63 (1), 61–72.
- Caselles, V., Sobrino, J.A., Coll, C., 1992. On the use of satellite thermal data for determining evapotranspiration in partially vegetated areas. *Int. J. Remote Sens.* 13 (14), 2669–2682.
- Chen, J.M., Rich, P.M., Gower, S.T., Norman, J.M., Plummer, S., 1997. Leaf area index of boreal forests: theory, techniques, and measurements. *J. Geophys. Res.* 102 (D24), 29429–29443.
- Cristobal, J., Poystos, R., Ninyerola, M., Llorens, P., Pons, X., 2011. Combining remote sensing and GIS climate modeling to estimate daily forest evapotranspiration in a Mediterranean mountain area. *Hydrol. Earth Syst. Sci.* 15 (5), 1563–1575.
- Curran, P.J., 1980. Multispectral remote sensing of vegetation amount. *Prog. Phys. Geogr.* 4 (3), 315–341.
- Feddema, J.J., Egbert, S.L., Park, S., 2005. MODIS land surface temperature composite data and their relationships with climatic water budget factors in the central Great Plains. *Int. J. Remote Sens.* 26, 1127–1144.
- Fisher, J.B., DeBiase, T.A., Qi, Y., Xu, M., Goldstein, A.H., 2005. Evapotranspiration models compared on a Sierra Nevada forest ecosystem. *Environ. Model. Softw.* 20 (6), 783–796.
- Glenn, E.P., Huete, A.R., Nagler, P.L., Hirschboeck, K.K., Brown, P., 2007. Integrating remote sensing and ground methods to estimate evapotranspiration. *Crit. Rev. Plant Sci.* 26 (3), 139–168.
- Hafeez, M.M., Chemin, Y., Van De Geisen, N., Bouman, B.A.M., 2002. Field evapotranspiration estimation in central Luzon, Philippines using different sensors: Landsat 7ETM+, terra modis, and aster. In: Proc., Symposium on Geospatial Theory, Processing, and Applications, Ottawa, Canada, 7 pp.
- Han, J., Kamber, M., 2001. Data Mining: Concepts and Techniques. Morgan Kaufmann Publishers, San Francisco, CA, USA.
- Haykin, S., 1999. Neural Networks: A Comprehensive Foundation, second ed. Prentice Hall, Inc., Upper Saddle River, NJ, USA.
- Hilker, T., Hall, F.G., Coops, N.C., Collatz, J.G., Black, T.A., Tucker, C.J., Grant, N., 2013. Remote sensing of transpiration and heat fluxes using multi-angle observations. *Remote Sens. Environ.* 137, 31–42.
- Huete, A.R., 1988. A soil-adjusted vegetation index (SAVI). *Remote Sens. Environ.* 25 (3), 295–309.
- Idso, S.B., Jackson, R.D., Reginato, R.J., 1975. Estimating evaporation: a technique adaptable to remote sensing. *Science* 189 (4207), 991–992.
- Jaramillo, F., Destouni, G., 2015. Local flow regulation and irrigation raise global human water consumption and footprint. *Science* 350 (6265), 1248–1251. <https://doi.org/10.1126/science.aad1010>.
- Jarecki, M.K., Lal, R., 2003. Crop management for soil carbon sequestration. *Crit. Rev. Plant Sci.* 22 (6), 471–502.
- Jensen, M.E., Burman, R.D., Allen, R.G. (Eds.), 1990. Evapotranspiration and Irrigation Water Requirements. ASCE Manuals and Reports on Eng. Manual of Practice No. 70. ASCE, New York.
- Johnson, D.M., 2016. A comprehensive assessment of the correlations between field crop yields and commonly used MODIS products. *Int. J. Appl. Earth Obs. Geoinf.* 52, 65–81.
- Justice, C.O., Vermote, E., Townshend, J.R.G., Defries, R., Roy, D.P., Hall, D.K., Salomonson, V.V., Privette, J.L., Riggs, G., Strahler, A., Lucht, W., Myneni, R.B., Knyazikhin, Y., Running, S.W., Nemani, R.R., Zhengming, W., Huete, A.R., Van Leeuwen, W., Wolfe, R.E., Giglio, L., Muller, J.-P., Lewis, P., Barnsley, M.J., 1998. The Moderate Resolution Imaging Spectroradiometer (MODIS): land remote sensing for global change research. *IEEE Trans. Geosci. Remote Sens.* 36 (4), 1228–1249.
- Kramer, S., Lavrač, N., Flach, P., 2001. Propositionalization approaches to relational data mining. In: Relational Data Mining. Springer, Berlin, Heidelberg, pp. 262–291.
- Kustas, W.P., Norman, J.M., 1996. Use of remote sensing for evapotranspiration monitoring over land surfaces. *Hydrol. Sci. J.* 41 (4), 495–516.
- Lal, R., 2004. Soil carbon sequestration impacts on global climate change and food security. *Science* 304 (5677), 1623–1627.
- le Maire, G., François, C., Soudani, K., Davi, H., Le Dantec, V., Saugier, B., Dufrêne, E., 2006. Forest leaf area index determination: a multiyear satellite-independent method based on within-stand normalized difference vegetation index spatial variability. *J. Geophys. Res.* 111 (G2), 13. <https://doi.org/10.1029/2005JG000122>.
- Lee, J.G., 1994. Counterspace Operations for Information Dominance. M.S. Thesis. The School of Advanced Airpower Studies, Maxwell Air Force Base, Alabama, U.S.A.
- Li, F., Lyons, T.J., 2002. Remote estimation of regional evapotranspiration. *Environ. Model. Softw.* 17 (1), 61–75.
- Li, Z.L., Tang, R., Wan, Z., Bi, Y., Zhou, C., Tang, B., Yan, G., Zhang, X., 2009. A review of current methodologies for regional evapotranspiration estimation from remotely-sensed data. *Sensors* 9 (5), 3801–3853.
- Liou, Y.A., Kar, S.K., 2014. Evapotranspiration estimation with remote sensing and various surface energy balance algorithms—a review. *Energies* 7 (5), 2821–2849.
- Long, D., Singh, V.P., 2013. Assessing the impact of end-member selection on the accuracy of satellite-based spatial variability models for actual evapotranspiration estimation. *Water Resour. Res.* 49 (5), 2601–2618.
- Majasalmi, T., Rautiainen, M., Stenberg, P., Manninen, T., 2015. Validation of MODIS and GEOV1 fPAR products in a boreal forest site in Finland. *Remote Sens.* 7 (2), 1359–1379.
- Majasalmi, T., Stenberg, P., Rautiainen, M., 2017. Comparison of ground and satellite-based methods for estimating stand-level fPAR in a boreal forest. *Agric. For. Meteorol.* 232, 422–432.
- Malone, R.W., Yagow, G., Baffaut, C., Gitau, M.W., Qi, Z., Amatya, D.M., Parajuli, P.B., Bonta, J.V., Green, T.R., 2015. Parameterization guidelines and considerations for hydrologic models. *Trans. ASABE (Am. Soc. Agric. Biol. Eng.)* 58 (6), 1681–1703.
- McCarthy, E.J., Skaggs, R.W., Farnum, P., 1991. Experimental determination of the hydrologic components of a drained forest watershed. *Trans. ASAE (Am. Soc. Agric. Eng.)* 34 (5), 2031–2039. <https://doi.org/10.13031/2013.31833>.
- Moran, M.S., Jackson, R.D., Raymond, L.H., Gay, L.W., Slater, P.N., 1989. Mapping surface energy balance components by combining Landsat Thematic Mapper and ground-based meteorological data. *Remote Sens. Environ.* 30, 77–87.
- Moran, M.S., Clarke, T.R., Inoue, Y., Vidal, A., 1994. Estimating crop water deficit using the relation between surface-air temperature and spectral vegetation index. *Remote Sens. Environ.* 49 (3), 246–263.
- Morris, J., Mann, L., Collopy, J., 1998. Transpiration and canopy conductance in a eucalypt plantation using shallow saline groundwater. *Tree Physiol.* 18 (8–9), 547–555.
- Muwamba, A., Amatya, D.M., Ssegane, H., Chescheir, G.M., Appelboom, T., Tollner, E.W., Nettles, J.E., Youssef, M.A., Birgand, F., Skaggs, R.W., Tian, S., 2015. Effects of site preparation for pine Forest/switchgrass intercropping on water quality. *J. Environ. Qual.* 44 (4), 1263–1272.
- Nghi, V.V., Dung, D.D., Lam, D.T., 2008. Potential evapotranspiration estimation and its effect on hydrological model response at the Nong Son Basin. *VNU J of Science, Earth Sciences* 24, 213–223.
- Noori, O., Panda, S.S., 2016. Site-specific management of common olive: remote sensing, geospatial, and advanced image processing applications. *Comput. Electron. Agric.* 127, 680–689. <https://doi.org/10.1016/j.compag.2016.07.031>.
- North, P.R.J., 2002. Estimation of fAPAR, LAI, and vegetation fractional cover from ATSR-2 imagery. *Remote Sens. Environ.* 80 (1), 114–121.
- Nouri, H., Beecham, S., Kazemi, F., Hassanli, A.M., 2012. A review of ET measurement techniques for estimating the water requirements of urban landscape vegetation. *Urban Water J.* 10 (4), 247–259.
- Olioso, A., Chauki, H., Courault, D., Wigneron, J.P., 1999. Estimation of evapotranspiration and photosynthesis by assimilation of remote sensing data into SVAT models. *Remote Sens. Environ.* 68 (3), 341–356.
- Olivera-Guerra, L.E., Merlin, O., Mattar, C., Durán-Alarcón, C., Santamaría-Artigas, A., Stefan, V., 2015. Combining meteorological and lysimeter data to evaluate energy and water fluxes over a row crop for remote sensing applications. In: 2015 IEEE International Geoscience and Remote Sensing Symposium (IGARSS), pp. 4649–4651.
- Panda, S.S., 2002. Data Mining Application in Production Management of Crop. Ph.D. Dissertation. North Dakota State University, Fargo, ND, USA, pp. 225–230.
- Panda, S.S., Hoogenboom, G., Paz, J., 2009. Distinguishing blueberry bushes from mixed vegetation land use using high resolution satellite imagery and geospatial techniques. *Comput. Electron. Agric.* 67 (1–2), 51–58.
- Panda, S.S., Ames, D.P., Panigrahi, S., 2010. Application of vegetation indices for agricultural crop yield prediction using neural network techniques. *Remote Sens.* 2 (3), 673–696.
- Panda, S.S., Amatya, D.M., Hoogenboom, G., 2014. Stomatal conductance, canopy temperature, and leaf area index estimation using remote sensing and OBIA techniques. *J. Spat. Hydrol.* 12, 1.
- Panda, S.S., Amatya, D.M., Sun, G., Bowman, A., 2016. Remote estimation of a managed pine forest evapotranspiration with geospatial technology. *Transactions of ASABE* 59 (6), 1695–1705.
- Panda, S.S., Amatya, D.M., Jackson, R., Sun, G., Noormets, A., 2018. Automated geospatial models of varying complexities for pine forest evapotranspiration estimation with advanced data mining. *Water* 10 (11), 1687. <https://doi.org/10.3390/w10111687>.
- Parrish, D.J., Fike, J.H., 2005. The biology and agronomy of switchgrass for biofuels. *Crit. Rev. Plant Sci.* 24 (5–6), 423–459.
- Paterson, A.H., Bowers, J.F., Feltus, F.A., 2008. Plant genetics and genomics: crops and models. In: Moore, P., Ming, R. (Eds.), *Genomics of Tropical Crop Plants*. Springer, New York, pp. 469–482.
- Pearcy, R.W., Schulze, E.D., Zimmermann, R., 1989. Measurement of transpiration and leaf conductance. In: Pearcy, R.W., Ehleringer, J.R., Mooney, H.A., Rundel, P.W. (Eds.), *Plant Physiological Ecology*. Springer, Dordrecht.
- Perrin, R.K., Vogel, K.P., Schmer, M.R., Mitchell, R.B., 2008. Farm-scale production cost of switchgrass for biomass. *Bioenerg. Res.* 1, 91–97.
- Pisek, J., Rautiainen, M., Nikopensius, M., Raabe, K., 2015. Estimation of seasonal dynamics of understory NDVI in northern forests using MODIS BRDF data: semi-empirical versus physically-based approach. *Remote Sens. Environ.* 163, 42–47.
- Pisek, J., Chen, J.M., Kobayashi, H., Rautiainen, M., Schaeppman, M.E., Karnieli, A., Sprinstin, M., Ryu, Y., Nikopensius, M., Raabe, K., 2016. Retrieval of seasonal dynamics of forest understory reflectance from semiarid to boreal forests using MODIS BRDF data. *J. Geophys. Res.: Biogeosciences* 121, 855–863. <https://doi.org/10.1002/2016JG003322>.
- Pottel, H., 2003. Statistical Flaws in Excel. Innogenetics NV, Technologiepark, vol. 6, 9052.
- Provoost, S., Van Til, M., Deronde, B., Knotters, A., 2005. Remote sensing of coastal vegetation in The Netherlands and Belgium. In: Herrier, J.-L., Mees, J., Salaman, A., Seys,

- J., Van Nieuwenhuysse, H., Dobbelaere, I. (Eds.), 2005. P. 139-149. Proceedings 'Dunes and Estuaries 2005' – International Conference on Nature Restoration Practices in European Coastal Habitats, Koksijde, Belgium, 19-23 September 2. 005, vol. 19 VLIZ Special Publication xiv + 685 pp.
- Rao, N.R., Garg, P.K., Ghosh, S.K., 2006. Estimation and comparison of leaf area index of agricultural crops using 1248 IRS LISS-III and 1249 EO-1 hyperion images. *J. of the Indian Society of Remote Sensing* 34 (1), 69–78.
- Rouse, J.W., Haas, R.H., Schell, J.A., Deering, D.W., 1973. Monitoring vegetation systems in the great plains with ERTS. In: *Third ERTS Symposium*, SP-351. NASA, Washington, D.C, pp. 309–317.
- Sack, L., Scoffoni, C., 2012. Measurement of leaf hydraulic conductance and stomatal conductance and their responses to irradiance and dehydration using the evaporative flux method (EFM). *J. Vis. Exp.: JoVE*. 70.
- Sahoo, K., Mani, S., Das, L., Bettinger, P., 2018. GIS-based assessment of sustainable crop residues for optimal siting of biogas plants. *Biomass Bioenergy* 110, 63–74.
- Sampson, D.A., Amatya, D.M., Blanton Lawson, C.D., Skaggs, R.W., 2011. Leaf area index (LAI) of loblolly pine and emergent vegetation following a harvest. *Trans. ASABE (Am. Soc. Agric. Biol. Eng.)* 54 (6), 2057–2066.
- Schellberg, J., Hill, M.J., Gerhards, R., Rothmund, M., Braun, M., 2008. Precision agriculture on grassland: applications, perspectives and constraints. *Eur. J. Agron.* 29 (2–3), 59–71.
- Senay, G.B., Bohms, S., Singh, R.K., Gowda, P.H., Velpuri, N.M., Alemu, H., Verdin, J.P., 2013. Operational evapotranspiration mapping using remote sensing and weather datasets: a new parameterization for the SSEB Approach. *J. Am. Water Resour. Assoc.* 49 (3), 1–15. <https://doi.org/10.1111/jawr.12057>.
- Simmons, B.A., Loque, D., Blanch, H.W., 2008. Next-generation biomass feedstocks for biofuel production. *Genome Biol.* 9, 242. <https://doi.org/10.1186/gb-2008-9-12-242>.
- Ssegane, H., Amatya, D.M., Muwamba, A., Chescheir, G.M., Appelboom, T., Tollner, E.W., Nettles, J.E., Youssef, M.A., Birgand, F., Skaggs, R.W., 2017. Calibration of paired watersheds: utility of moving sums in presence of externalities. *Hydrol. Proced.* 31 (20), 3458–3471. <https://doi.org/10.1002/hyp.11248>.
- Sterling, S.M., Ducharme, A., Polcher, J., 2013. The impact of global land-cover change on the terrestrial water cycle. *Nat. Clim. Chang.* 3 (4), 385–390. <https://doi.org/10.1038/nclimate1690>.
- Sun, G., Alstad, K., Chen, J., Chen, S., Ford, C.R., Lin, G., Liu, C., Lu, N., McNulty, S.G., Miao, H., Noormets, A., Vose, J.M., Wilske, B., Zeppel, M., Zhang, Y., Zhang, Z., 2011. A general predictive model for estimating monthly ecosystem evapotranspiration. *Ecohydrology* 4, 245–255. <https://doi.org/10.1002/eco.194>.
- Tao, X., Liang, S., Wang, D., 2015. Assessment of five global satellite products of fraction of absorbed photosynthetically active radiation: intercomparison and direct validation against ground-based data. *Remote Sens. Environ.* 163, 270–285.
- Tian, S., Youssef, M.A., Skaggs, R.W., Amatya, D.M., Chescheir, G.M., 2012. DRAINMOD-Forest: integrated modeling of hydrology, soil carbon, and nitrogen dynamics, and plant growth for drained forest. *J. Environ. Qual.* 41, 764–782.
- Tian, F., Qiu, G., Yang, Y., Lü, Y., Xiong, Y., 2013. Estimation of evapotranspiration and its partition based on an extended three-temperature model and MODIS products. *J. Hydrol.* 498, 210–220.
- Turner, D.P., Cohen, W.B., Kennedy, R.E., Fassnacht, K.S., Briggs, J.M., 1999. Relationships between leaf area index and Landsat TM spectral vegetation indices across three temperate zone sites. *Remote Sens. Environ.* 70 (1), 52–68.
- van der Ploeg, M., de Rooij, G., 2014. Observing plants dealing with soil water stress: daily soil moisture fluctuations derived from polymer tensiometers. In: *EGU General Assembly Conference Abstracts*, vol. 16. pp. 6491.
- Vásquez, V., Thomsen, A., Iversen, B.V., Jensen, R., Ringgaard, R., Schelde, K., 2015. Integrating lysimeter drainage and eddy covariance flux measurements in a groundwater recharge model. *Hydrol. Sci. J.* 60 (9), 1520–1537.
- Verger, A., Baret, F., Weiss, M., Filella, I., Peñuelas, J., 2015. GEOCLIM a global climatology of LAI, FAPAR, and FCOVER from VEGETATION observations for 1999–2010. *Remote Sens. Environ.* 166, 126–137.
- Viessman, W., Lewis, G.L., 2003. *Introduction to Hydrology*. Prentice Hall, Upper Saddle River, NJ, pp. 344p.
- Wang, H., Jia, G., 2013. Regional estimates of evapotranspiration over Northern China using a remote-sensing-based triangle interpolation method. *Adv. Atmos. Sci.* 30 (5), 1479–1490.
- Wang, L., Qu, J.J., 2009. Satellite remote sensing applications for surface soil moisture monitoring: a review. *Front. Earth Sci. China* 3 (2), 237–247.
- Weigand, C.L., Bartholic, J.F., March 1970. Remote sensing in evapotranspiration research on the Great Plains. In: *Proceedings of the Great Plains Agricultural Council Evapotranspiration Seminar*, Bushland, TX, USA, pp. 137–180.
- Yang, Y., Shang, S., 2013. A hybrid dual-source scheme and trapezoid framework-based evapotranspiration model (HTEM) using remotely-sensed images: algorithm and model test. *J. Geophys. Res. Atmos.* 118 (5), 2284–2300.
- Yang, W., Kobayashi, H., Suzuki, R., Nasahara, K.N., 2014a. A simple method for retrieving understory NDVI in sparse needle-leaf forests in Alaska using MODIS BRDF data. *Remote Sens.* 6 (12), 11936–11955.
- Yang, W., Kobayashi, H., Suzuki, R., Nasahara, K.N., 2014b. A simple method for retrieving understory NDVI in sparse needle leaf forests in Alaska using MODIS BRDF data. *Remote Sens.* 6 (12), 11936–11955.
- Zhang, K., Kimball, J.S., Running, S.W., 2016. A review of remote sensing based actual evapotranspiration estimation. *Wiley Interdisciplinary Reviews: Water* 3 (6), 834–853.